

Temporal processing and context dependency in *C. elegans* mechanosensation

Mochi Liu¹, Anuj K Sharma², Joshua W Shaevitz^{1,2}, Andrew M Leifer^{2,3*}

*For correspondence:
leifer@princeton.edu (AML)

¹Lewis-Sigler Institute for Integrative Genomics, Princeton University, USA; ²Department of Physics, Princeton University, Princeton University, USA; ³Princeton Neuroscience Institute, Princeton University, USA

Abstract A quantitative understanding of how sensory signals are transformed into motor outputs places useful constraints on brain function and helps reveal the brain's underlying computations. We investigate how the nematode *C. elegans* responds to time-varying mechanosensory signals using a high-throughput optogenetic assay and automated behavior quantification. In the prevailing picture of the touch circuit, the animal's behavior is determined by which neurons are stimulated and by the stimulus amplitude. In contrast, we find that the behavioral response is tuned to temporal properties of mechanosensory signals, like its integral and derivative, that extend over many seconds. Mechanosensory signals, even in the same neurons, can be tailored to elicit different behavioral responses. Moreover, we find that the animal's response also depends on its behavioral context. Most dramatically, the animal ignores all tested mechanosensory stimuli during turns. Finally, we present a linear-nonlinear model that predicts the animal's behavioral response to stimulus.

Introduction

An animal's nervous system interprets sensory signals to guide behavior, including to evade predation. Temporal properties of a stimulus can be important for determining an animal's behavioral response. For example, mice exhibit defensive behaviors in response to looming visual stimuli that increase in size, but not to similar stimuli that decrease in size (*Yilmaz and Meister, 2013*). Investigating how the nervous system processes these signals is a critical step towards understanding neural function.

Mechanosensation in the nematode *Caenorhabditis elegans* is an attractive platform for investigating sensorimotor processing. Six soft-touch mechanosensory neurons arranged throughout the body detect mechanical stimuli delivered by a small probe in what is called a touch, or by striking the petri dish containing the animal in what is called a tap (*Chalfie and Sulston, 1981*). In the prevailing picture of the touch circuit, the animal's behavior is determined entirely by which neurons are stimulated and by the stimulus amplitude. Despite decades of investigation, however, the behavioral response to dynamic time-varying mechanosensory signals has not been fully explored.

Here we revise the prevailing picture of the mechanosensory response system by quantitatively exploring the animal's detailed behavioral response to rich, dynamically varying signals. In contrast to the prevailing picture, we find that the animal responds to temporal features of signals in its mechanosensory neurons, like its time-derivative, that extend over many seconds. Moreover, we find evidence that the animal's sensorimotor response depends on the animal's current behavior

arXiv:1803.04085v2 [q-bio.NC] 20 Mar 2018

state. That we find temporal processing and context dependency even in the nematode's relatively simple touch circuit, raises the possibility that these features could be ubiquitous across sensory systems. Finally, we present a simple quantitative model that predicts the animal's response to novel mechanosensory signals.

Mechanosensation is important for *C. elegans* survival. *C. elegans* are preyed upon by nematophagous fungi, and touch-defective animals fail to detect and escape from the fungus (*Maguire et al., 2011*). Much is already known about this critical circuit. The six soft-touch mechanosensory neurons detect both spatially localized and non-localized stimuli. Anterior touches are detected by anterior neurons ALML, ALMR and AVM and evoke reversal behaviors while posterior touches are detected by posterior neurons PLML and PLMR and evoke forward sprints (*Chalfie and Sulston, 1981; Chalfie et al., 1985; Mazzochette et al., 2018*). Non-spatially localized plate taps are detected by both anterior and posterior soft-touch neurons and evoke reversals (*Chalfie and Sulston, 1981; Rankin et al., 1990*) and, on rare occasions, forward acceleration (*Wicks and Rankin, 1995; Chiba and Rankin, 1990*). Due in part to its ease of delivery, and its inherent compatibility with high-throughput methods (*Swierczek et al., 2011*), plate tap has emerged as an assay for studying sensitization and habituation (*Rankin et al., 1990*) and the development, circuitry (*Chalfie and Sulston, 1981*), genes, molecules and receptors (*Sanyal et al., 2004; Kindt et al., 2007*) of the mechanosensory system.

When the animal interacts with its environment or brushes up against a nematophagous fungi's constricting ring, it inherently receives time-varying stimuli. An individual touch receptor neuron's response to force is well characterized (*O'Hagan et al., 2005*), including to time varying stimuli (*Eastwood et al., 2015*). The onset and offset of an applied force evokes strong excitatory currents that adapt on a few tens of milliseconds timescale and have a frequency response thought to peak in the 100 Hz regime (*Eastwood et al., 2015*). In contrast to the detailed understanding at the single neuron level, the animal's downstream response to rich temporally varying mechanosensory signals has not been explored.

The animal's behavior response to mechanosensory stimuli has primarily been studied in response to impulse stimuli. These are brief applications of touch, tap or optogenetic stimulation whose most salient feature is the stimulus amplitude, not its temporal profile. In the classical touch assay, for example, a saturating force is applied lasting a few tenths of a second (*Nekimken et al., 2017*). Tap stimuli are even shorter in duration. In impulse-like experiments, it is the stimulus amplitude (force, indentation or optogenetic intensity) that determines behavioral response (*Petzold et al., 2013; Stirman et al., 2011; Mazzochette et al., 2018*). To our knowledge, the only work investigating behavioral responses to temporally varying stimuli involves trains of taps or touches (*Chiba and Rankin, 1990; Kitamura et al., 2001*), trains of optogenetic pulses (*Porto et al., 2017; Leifer et al., 2011*) or the delivery of a 1 kHz acoustic vibration (*Nagy et al., 2014a,b*).

Similarly, the quantification of behavior responses to these stimuli have focused on a few behaviors that were chosen *a priori*, and usually related to reversals. Early work scored the animal's reversals (*Chiba and Rankin, 1990*) and accelerations (*Wicks and Rankin, 1995*) and more recent work includes reversal distance (*Kitamura et al., 2001*), rate of reversals (*Swierczek et al., 2011*) or pauses, reversal duration and reversal latency (*Ardiel et al., 2017*). Yet the animal's repertoire of behavior is known to be larger (*Stephens et al., 2008; Brown et al., 2013*).

The picture that emerges from these studies is one where behavior depends solely on the set of neurons stimulated and the stimulus strength. The location of an applied force determines which touch receptor neurons are activated and thus whether the animal accelerates or reverses, while the amplitude of the applied stimulus determines the probability that the animal responds at all (*Driscoll and Kaplan, 1997; Petzold et al., 2013; Mazzochette et al., 2018*). Now, however, this picture is coming under greater scrutiny. Recently, Porto et al. report the use of reverse correlation and a binary optogenetic stimulus to present evidence that temporal processing is important for the animal's behavioral response (*Porto et al., 2017*). In our work here, we show that the nervous system processes signals from the mechanosensory neurons as a timeseries over many seconds.

We find that the animal's behavior response depends on higher order temporal features like the derivative of those mechanosensory signal, and also depends on the animal's own behavioral context.

Here we revisit the animal's behavioral response to mechanosensory stimulation armed with high-throughput optogenetic methods for delivering time varying stimuli and improved techniques for measuring animal posture (*Stephens et al., 2008*) and behavior (*Berman et al., 2014*). Using reverse correlation (*Ringach and Shapley, 2004; Schwartz et al., 2006; Gepner et al., 2015*) we analyze over 8,000 animal-hours of recordings (three orders of magnitude greater than previous investigations) and find new insights into the interplay between sensory processing and behavior.

Results

Mechanosensation evokes a range of behavioral responses

We first investigated the animal's response to plate tap, a spatially non-localized mechanosensory stimulus generated by tapping the dish containing the animals. Plate taps had previously been reported to evoke reverse locomotion (*Rankin et al., 1990*) and rarely forward accelerations (*Wicks and Rankin, 1995*). A solenoid repeatedly delivered a tap stimulus every 60 seconds for 30 minutes to a plate of many Wild-Type (N2) worms, repeated across 22 plates, resulting in 40,409 total animal-tap presentations. The inter-stimulus interval was chosen to minimize effects of habituation (*Rankin and Wicks, 2000*). The animal's behavior was continuously measured and classified using a behavior mapping technique similar to (*Berman et al., 2014*). Briefly, statistical inference was performed on all of the animal's posture dynamics to generate a single behavior map. Stereotyped posture dynamics that emerged from this map were defined as behaviors. Each individual animal's posture dynamics were projected into this map at each point in time and automatically classified into one of 9 behavior states that were assigned labels such as Turn. See *Figure 1*, and *Figure 1 - Figure Supplements 1 and 2* and methods for a complete description of the behavior mapping. Also see example videos of behavioral mapping in *Figure 1 - Figure Supplements 3 and 4*.

Consistent with previous reports, we observe that taps most dramatically evoke the animal to transition to the Fast Reverse state. Tap stimulus induced a 14-fold increase in the fraction of animals exhibiting Fast Reverse immediately post stimuli, see *Figure 2a* and *2 - Figure Supplement 2*. Additionally, animals that continued in forward locomotion exhibited an overall slowing down, transitioning from fast locomotion states to slower locomotion states, which to our knowledge had not previously been reported. We also observed a 4.5 fold increase in the fraction of animals exhibiting Turn behavior approximately 5 seconds post stimulus. The fraction of animals exhibiting Slow Reverse also increased slightly upon stimulation. These measurements suggest that plate tap evokes a wide-range of behavioral responses in the animal.

Optogenetic stimulation mimics tap

We sought to activate the mechanosensory circuit optogenetically because optogenetic stimulation is more amenable to modulation and control. Optogenetic stimulation of the six mechanosensory neurons had previously been shown to evoke reversals and accelerations, similar to tap (*Nagel et al., 2005*). We wondered whether the details of the behavior response to tap that we observed are also present in response to optogenetic activation. Animals expressing the light gated ion channel Chrimson in the soft touch mechanosensory neurons (strain AML67 [*Pmec-4::Chrimson4.2::SL2::mCherry::unc-54*]) were illuminated with red light for 1 second with a 60 second inter-stimulus interval (2,444 stimulus-animal presentations, 20 $\mu\text{W}/\text{mm}^2$, selected to be in a region of high behavior sensitivity, see *Figure 2c*). Consistent with previous reports, light stimulation evoked a behavior response that was quantitatively similar to that of the plate tap, see *Figure 2b* and required the cofactor all-trans retinal (ATR) *2-Figure supplement 3*. For both light and tap, the most salient response was a dramatic increase in animals in Fast Reverse. Both light and tap also evoked an increase in occupancy in Forward 3 and both evoked similar decreases in Forward 4, 5

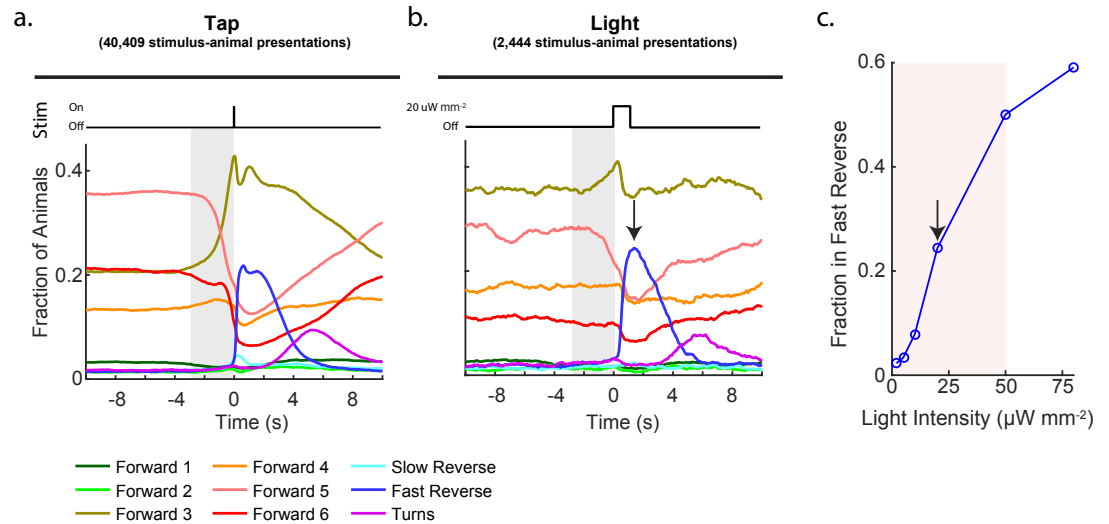


Figure 2. Stimulation evokes a diverse range of behavior responses. **a.)** Fractions of animals occupying each behavior state are shown in response to a plate tap (40,409 stimulus-animal presentations) and **b.)** in response to a 1 second optogenetic light stimulation of the six soft touch mechanosensory neurons (2,444 stimulus-animal presentations, $20 \mu\text{W mm}^{-2}$). Note the similarity in the behavior responses for light and tap. Gray shaded window indicates inherent temporal uncertainty in behavior classification. See methods. **c.)** Response to optogenetic stimulation depends on light intensity. Peak fraction of animals in the Fast Reverse state in a 6 second window post stimulus are shown for different intensity light pulses. More than 2,000 stimulus-animal presentations were recorded for each point plotted. Arrow indicates light intensity used in **b.** Pink shaded region indicates light range used for subsequent continuous light stimulation experiments, as in **Figure 3.**

Figure 2-Figure supplement 1. Diagram of high-throughput stimulation and behavior assay.

Figure 2-Figure supplement 2. Transition rates for tap and light stimulation.

Figure 2-Figure supplement 3. Control animals grown without ATR are light insensitive.

Figure 2-Figure supplement 4. Tap sensitivity of transgenic animals is reduced compared to wildtype.

and 6. Both light and tap also evoked an increase in Turns that peaked 5 seconds post-stimulus. Hence, optogenetic stimulation of mechanosensory neurons evoke detailed behavior responses similar to that of a mechanical stimulus. This suggests that our optogenetic stimulation generates physiologically reasonable signals in the mechanosensory neurons and we therefore proceeded to explore the animal's response to optogenetic stimulation.

Behavioral responses are correlated to temporal features like the derivative

When the animal explores its natural environment, crawls through crevices, and interacts with other organisms, it likely experiences time varying mechanical stimuli. Therefore we sought to investigate the animal's response to random temporally varying optogenetic stimulation. We find that the animal's specific behavioral response correlates with higher order temporal features of the stimulus, not merely the amplitude.

To deliver rich temporally varying stimuli, we continuously presented a plate of transgenic animals with light modulated by broad frequency noise (7 Hz nyquist limit, 0.5 s correlation time, $25 \mu\text{W mm}^{-2}$ average intensity, min 0, max $50 \mu\text{W mm}^{-2}$, see power spectra **Figure 3** - Figure Supplement 4). Noise stimulation evoked a wide range of behavioral responses, see **Figure 3** - Figure Supplement 1. We used reverse correlation to identify the salient features of the stimulus that correlates with transitions into each behavior. Reverse correlation yields kernels that describe how a behavior is tuned to a stimulus. Kernels are particularly powerful in the context of the linear non-linear (LN) model, a ubiquitous model in neuroscience that can be used to predict a nervous systems' stimulus response (*Ringach and Shapley, 2004; Schwartz et al., 2006; Coen et al.,*

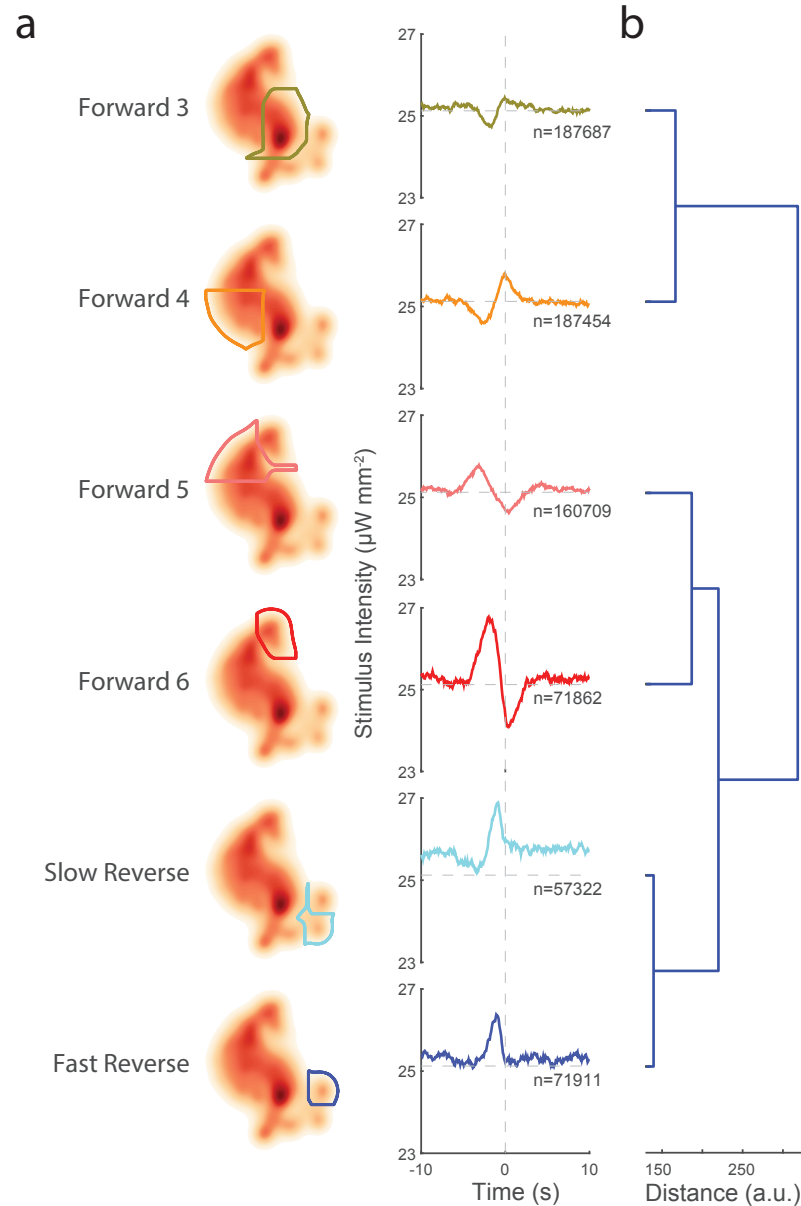


Figure 3. Transitions into behavior states are tuned to higher order temporal features of the stimulus like the derivative. **a.)** Random noise time-varying light stimulus is delivered to a population of animals. Behavior-triggered averages (also referred to as kernels) are calculated for transitions into each behavior state from 1,784 animal-hours of recordings. Each behavior triggered average describes features of the stimulus that correlate with that behavior transition. Only those behavior triggered averages that pass a significance test compared to a shuffled stimuli are shown. The shape of the behavior triggered average depends on the behavior. Note that some behaviors have gaussian like shapes, while others have biphasic shapes that act like derivatives. The number of observed transitions, n , into each behavior is listed. **b.)** Similar behaviors have similar behavior-triggered averages. Hierarchical clustering was performed on the euclidian distance of the scaled behavior-triggered averages. Dendrogram is shown. The two reversal states, for example, form a cluster.

Figure 3-Figure supplement 1. Change in behavioral occupancy evoked by random noise stimulation.

Figure 3-Figure supplement 2. Behavior triggered averages and non-linearities for all behaviors.

Figure 3-Figure supplement 3. Behavior triggered averages for control animals grown without ATR.

Figure 3-Figure supplement 4. Power spectra of a single instantiation of the random noise stimulus.

2014; Gepner et al., 2015; Hernandez-Nunez et al., 2015; Calhoun and Murthy, 2017; Clemens and Murthy, 2017). See in particular (Gepner et al., 2015). Briefly, the LN model treats the response to a stimulus as a stochastic process involving two steps: first the stimulus timeseries $s(t)$ is convolved with a kernel A (linear operation), and then it is transformed into a response probability P via a non-linear look-up function f (non-linear operation), such that,

$$P[\text{behavior}](t) = f[(A * s)(t)]; \quad (A * s) = \int_0^{\infty} A(\tau)s(t - \tau)d\tau. \quad (1)$$

The shape of the kernel and non-linearity describes how a behavior response is tuned to the stimulus.

Kernels can be estimated by finding the behavior triggered average. Briefly, the stimulus in a time window centered on a behavior transition is averaged across all such behavior transitions. The mean subtracted and time-reversed behavior triggered average is an estimate of the kernel and so henceforth we use the terms behavior triggered average and kernel interchangeably. Once the kernels A are calculated, it is straightforward to estimate the non-linearities f from the observed behavior responses (see methods). Kernels and associated non-linearities were computed for transitions into each of the 9 behavior states from over 50,000 behavior transition events per behavior, see **Figure 3** and **Figure 3** - Figure Supplement 2. Kernels for 6 of the 9 behaviors were found to be significant compared to a shuffled stimuli (see methods). In contrast, kernels computed from control animals grown without all-trans retinal all failed to pass our significance threshold, see **Figure 3** - Supplementary Figure 3. Non-linearities calculated for the 6 behaviors were found to be mostly linear, suggesting that in our case the kernels themselves capture most of the information about how the nervous system responds to our stimulus.

Our prior understanding of the mechanosensory circuit makes strong predictions about the shape of the kernels that we should observe. If behavior depends only on which neurons are activated, then all kernels should have the same shape, scaled linearly, because we are always activating the same set of neurons. (This assumes all six neurons are activated in a linear regime, which seems reasonable given the approximately linear response observed in **Figure 2c**). Moreover, if the probability of response depends only on instantaneous stimulus amplitude, then we further expect all kernels to be narrow gaussians. In contrast to these predictions, we see a wide diversity of kernels. Forward locomotion kernels have biphasic waveforms, not at all like gaussians. Forward 6, for example has the shape of a differentiator suggesting that the transitions into Forward 6 correlate with decreasing stimuli on a 7 second timescale. Kernels for Slow Reverse and Fast Reverse, on the other hand, do look like gaussians, consistent with the interpretation that *reversals* do depend on the stimulus amplitude. Interestingly, the gaussians are wide, which suggests that the animal may integrate sensory signal over three to four seconds in determining to reverse.

Taken together, we conclude that the animal's behavior response is not merely correlated with which neurons are stimulated and the stimulus amplitude. Instead different behaviors correlate with different temporal features of signals in the mechanosensory neurons, even though the same six neurons were always activated. The behavioral response correlates with properties of the stimulus like the derivative or the integral, not just the amplitude.

Similar behavioral responses are tuned to similar stimuli

We wondered about the organization of the behavioral responses with respect to the stimuli to which they are tuned. Ethologically, one might expect animals to have evolved their behavioral response so that similar behaviors are tuned to similar stimuli. Indeed, we find that similar behaviors have quantitatively similar kernels. Hierarchical clustering was performed on the euclidian distance of the scaled kernels, see **Figure 3**. The two reverse locomotion states have similar kernels and were clustered together. Forward velocity states fell into two clusters based on speed: Forward 3 and Forward 4 are slower and clustered together, while Forward 5 and Forward 6 are faster and clustered together. That similarities in the kernels reflect similarities of their associated behaviors, provides additional confidence in our reverse correlation analysis.

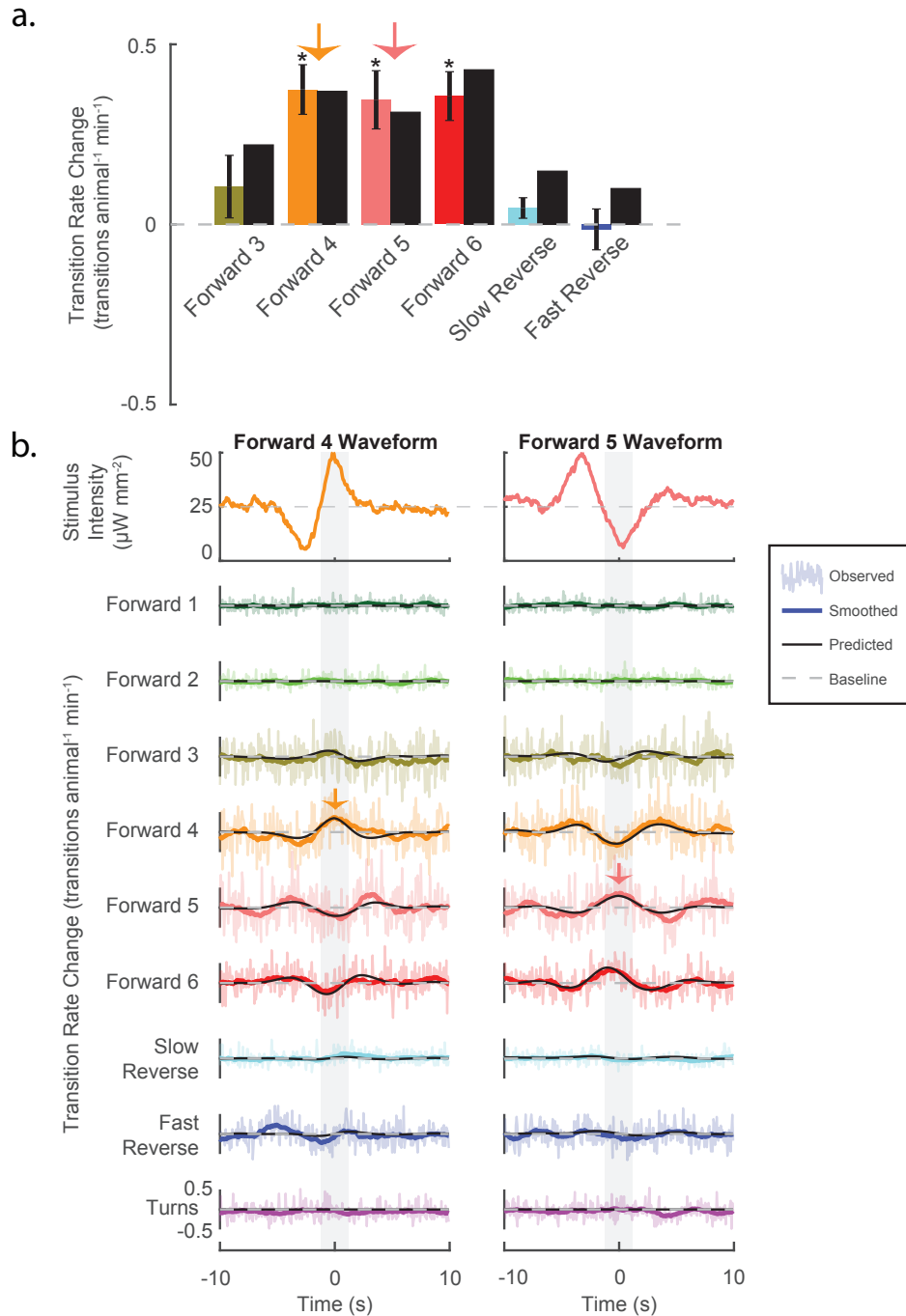


Figure 4. Stimuli can be tailored to elicit specific behavioral responses, and the LN model predicts such responses. **a.)** Animals are presented with stimuli shaped like the kernels in *Figure 3*. Predicted (black bar) and observed (color bar) changes in transition rate are shown for transitions into each kernel-shaped stimulus' corresponding behavior. For example, a Forward 3 shaped stimulus increases transitions into Forward 3 (mustard bar). For five of six behaviors, stimulation evoked increased transitions into their corresponding behaviors, as predicted. Transition rate changes are measured with respect to baseline (see methods). Significance is estimated via a t-test and error bars show standard error of the mean. The number of stimulus-animal presentations, from left to right, were {14,238, 13,612, 14,699, 14,424, 14,194, 13,708}. Of these, the number of timely transitions observed were {1,400, 1,428, 1,692, 944, 191, 513}. The p-values were { $2.2 \cdot 10^{-1}$, $5.6 \cdot 10^{-6}$, $1 \cdot 10^{-4}$, $3.4 \cdot 10^{-5}$, $7.5 \cdot 10^{-2}$, $9.5 \cdot 10^{-1}$ }. **b.)** The LN model predicts details of the animal's behavioral response. For each point in time, the LN model predicts the change from baseline of transition rates for all nine behaviors in response to a stimulus. Detailed responses to Forward 4- and Forward 5-kernel-shaped stimuli are shown (see *Figure 4* - Figure Supplement 1 for the rest). Raw transition rates (light colored shading), smoothed transition rates (colored line) and LN prediction (solid black line) are shown. For stimuli shaped like Forward 4, the LN model correctly predicts not only that transitions into Forward 4 increase, but also that transitions into Forward 5 and 6 decrease. Light gray shading indicates the 2 s time window used to calculate transition rates for the transitions shown in **a** (orange and pink arrows). Of 13,612 and 14,699 presentations for Forward 4- and 5-kernel shaped stimuli, respectively, the following number of transitions were observed in the 20 second window, by row for Forward 4-shaped: {1,265, 1,330, 12,312, 11,962, 13,436, 6,861, 1,735, 4,934, 2,864} and for Forward 5-shaped {1,198, 1,437, 13,657, 13,538, 14,656, 7,295, 1,673, 5,506, 3,118}.

Figure 4-Figure supplement 1. Behavioral responses to all kernel-shaped stimuli.

Figure 4-Figure supplement 2. Control animals grown without ATR do not respond to kernel-shaped stimulus.

Stimuli can be tailored to generate specific behavioral responses

To causally test whether specific signals in the mechanosensory neurons can bias the animal towards specific behaviors as predicted, we generated stimuli that were tailored to elicit specific behavioral responses. The kernels found in **Figure 3** purport to describe how each behavioral response is tuned to stimuli. Therefore, stimuli shaped like one of the kernels should drive an *increase* in transitions into its respective behavior. If, however, the behavioral response is tuned differently, then the kernel-shaped stimulus may evoke *decreases* in transitions to that behavior. (We already know that the animal can respond to some stimuli by decreasing transitions to certain behaviors because we saw this with tap and Forward 6, for example, see **Figure 2** - Figure Supplement 2).

We tested whether stimuli shaped like the kernels in **Figure 3** increased transitions into its associated behaviors. Kernel waveforms were presented to a plate of animals in a randomized order (6 kernels, >13,500 animal-stimulus presentations per kernel; 40 s inter-stimulus interval). Five of six kernels elicited increased transitions to their respective behaviors as predicted, three of the six significantly so, see **Figure 4a**. None significantly decreased transitions to their respective behaviors. We therefore conclude that the kernels correctly depict tuning of the behavioral responses. Consequently we conclude that mechanosensory signals (even in the same neurons) can be tailored to evoke specific behaviors just by altering the stimulus waveform.

LN model predicts behavioral response, including to novel stimuli

The LN model provides an analytical framework to predict how an animal responds to a stimulus. The LN model correctly predicted that kernel shaped waveforms should increase transitions into each kernel's associated behavior state, see **Figure 4a**. The kernel-shaped waveforms also evoked other behavioral responses. For example, stimuli shaped like the Forward 4 kernel increased transitions to both Forward 4 and Forward 3; but decreased transitions to Forward 5 and 6, see **Figure 4b**. How well, we wondered, does the LN model predict those responses? We compared the observed behavioral responses (colored lines) to detailed time-dependent predictions made by the LN model (black lines). To the resolution with which we could observe, we were reassured to find that the LN model correctly predicted the sign and temporal profile of changes in transition rates for all nine behavior states in response to each of the six kernel stimuli **Figure 4b** and **Figure 4** - Figure Supplement 1, suggesting that the LN model captures myriad details of the animal's behavioral response.

We further challenged our understanding of the animal's behavioral response to stimulus by presenting an entirely novel stimulus, a triangle-wave (340,757 stimulus-animal presentations), see **Figure 5** and **Figure 5** - Figure supplement 1. How well does the LN model predict the animal's behavior response to this novel stimulus? The LN model captured the sign and general trend (though not all features) of the time-dependent change in the transition rate to all nine behaviors in response to the triangle wave. Moreover, the LN model provides a framework for understanding the animal's response by inspecting features of the kernel waveform. For example, the Fast Reverse kernel is symmetric in time and its mean-subtracted integral is positive. Therefore the shape of the Fast Reverse kernel suggests that Fast Reverse should be tuned to the overall stimulus intensity but not its derivative. Indeed we observe a very slight increase in the rate of transitions to Fast Reverse during peak stimulus intensity. Conversely the Forward 6 kernel is asymmetric in time and its biphasic waveform resembles that of the negative derivative of a gaussian. Therefore Forward 6 should be tuned to decreases in stimulus intensity, as we observe.

Taken together, our experiments show that the animal can be driven to transition into different specific behavior states by modulating the temporal profile of signals in the same mechanosensory neurons, and that the LN model predicts the animal's response.

Sensory processing is context dependent

C. elegans is known to respond differently to the same stimuli when it is in different long-lived behavior states like hunger (**Ghosh et al., 2016**), or quiescence (**Schwarz et al., 2011; Nagy et al.,**

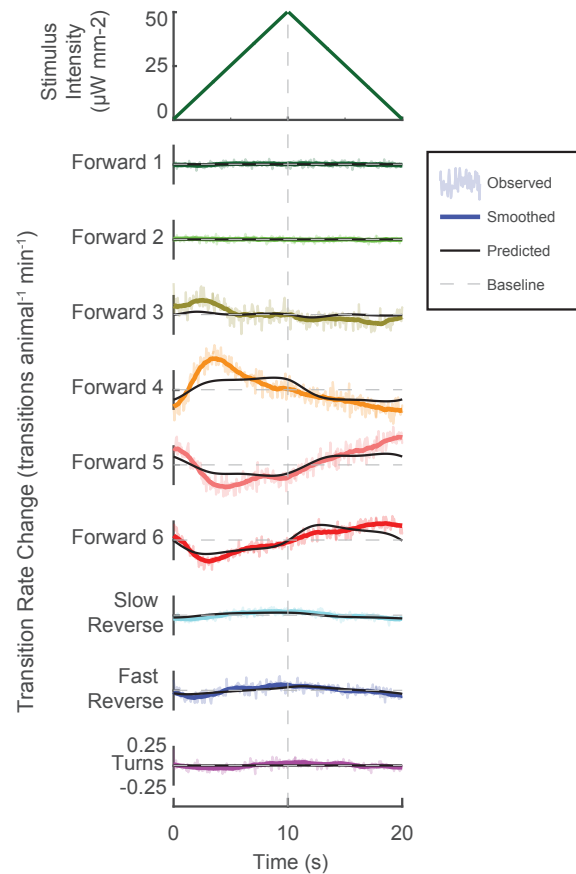


Figure 5. Novel stimuli can be constructed to enrich specific mechanosensory responses. A novel triangle-wave optogenetic light stimulus was repeatedly presented to animals. Change in transition rates are shown for transitions into each behavior (raw, light color shaded; smoothed, solid color line). Changes to transition rate as predicted by the LN model are also shown (black line). Increasing light intensity increases transitions into Forward 3 and 4, while decreasing light intensity increases transitions into Forward 5 and 6. Transitions into Slow and Fast Reverse are highest during highest stimulus intensity. The LN model predicts these trends (though not all the details) despite never previously experiencing this particular stimulus. Of 340,757 animal-stimulus presentations the following number of transitions were observed (by row, from top to bottom): {33,315, 31,243, 298,400, 343,474, 327,509, 160,332, 43,909, 106,743, 57,439}.

Figure 5-Figure supplement 1. Control animals grown without ATR do not respond to triangle wave stimuli.

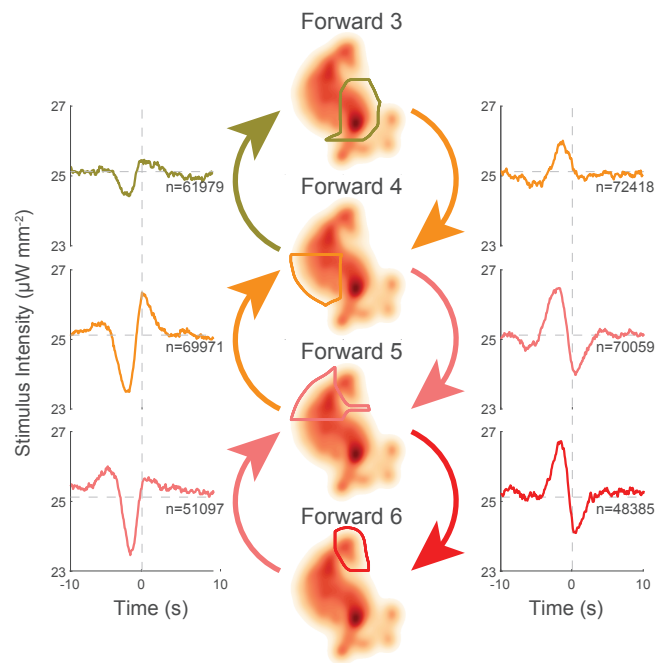


Figure 6. Behavior transitions that involve slowing down and speeding up have stereotyped tuning. Selected context-dependent kernels are shown for transitions amongst forward locomotory states, where higher numbered states have higher velocities. Kernels for slowing transitions (left column) are all similar, while kernels for speeding up transitions (right column) are also similar. Slowing and speeding-up kernels resemble horizontal reflections of one another.

Figure 6-Figure supplement 1. All 72 pairwise context-dependent behavior triggered averages.

Figure 6-Figure supplement 2. All 72 pairwise context-dependent behavior triggered averages for control animals grown without ATR.

2014b) and arousal (Cho and Sternberg, 2014). We wondered whether mechanosensory processing might additionally be influenced by short-lived behavior states, like the Turn, Reverse or Forward locomotory states measured here. To investigate tuning of the animal's behavioral response conditional on its current behavior state, we calculated context-dependent kernels, one for each pairwise transition, see Figure 6 - Figure supplement 1. Of 72 possible pairwise transitions, 27 had kernels that passed our shuffled significance threshold (compared to only 4 for our off-retinal control, see Figure 6 - Figure Supplement 2). Transitions to some behavior states, like Forward 4, had kernels that changed dramatically depending on which behavior the animal originated from, see columns in Figure 6 - Figure Supplement 1. The pairwise-specific kernels provided evidence of two types of context-dependent sensory processing in *C. elegans* that occur on short-time scales. In both cases the animal appears to respond to the same stimuli differently depending on its current behavior. In the first, the animal responds to certain mechanosensory signals by speeding up or slowing down. In the second type, the animal suppresses its response to mechanosensory stimuli during turning behavior. These two types of context-dependency are described below.

There are mechanosensory signals for speeding up or slowing down

Behavior transitions that involve slowing down have similar tuning. For example, the Forward 5→4 kernel has a similar shape to the Forward 4→3 kernel, see Figure 6, left column. Likewise, transitions involving speeding up also have similar kernels. For example, Forward 3→4 and Forward 4→5 have similar kernels, see Figure 6, right column. Moreover, the two classes of kernels appear to be reflections of one another about the line of mean stimulus intensity. The stereotypy of the speed up and slow down kernels suggests that the animal has evolved to respond to certain stimuli

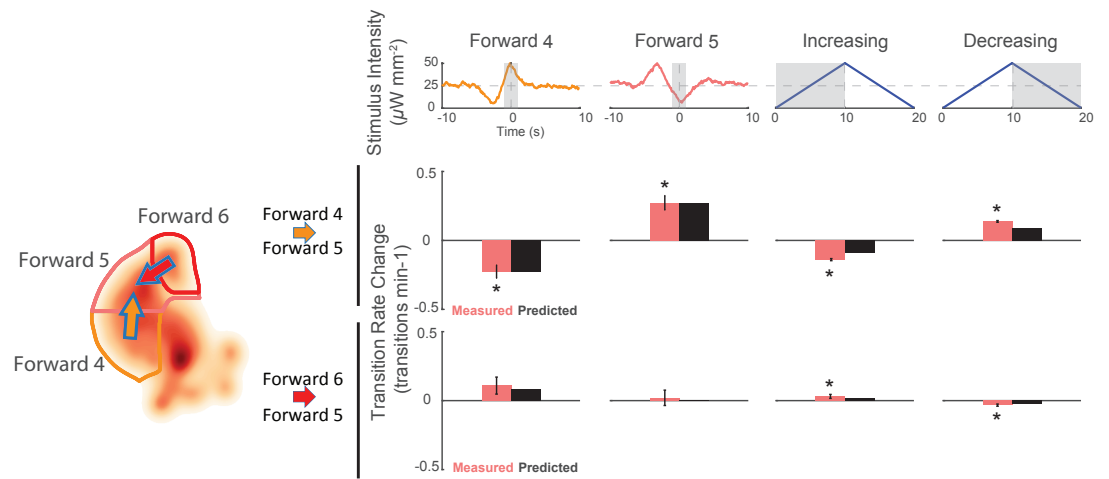


Figure 7. Animals respond to the same stimuli differently depending on their current behavior state. The change in transition rate from baseline is shown for transitions into Forward 5 from either Forward 4 (middle row) or Forward 6 (bottom row) in response to four different stimuli (columns). Observed transition rates (colored bars) are compared to LN model predictions (black bars). The stimulus effects the rate of transitions into Forward 5 differently depending on whether the animal was in Forward 4 or Forward 6 at the time of stimulus. For example, consistent with the animal responding to a slowing down signal, the Forward 4-shaped stimulus decreases Forward 4→5 transitions, but increases Forward 6→5 transitions. Star indicates significant change in transition rate from baseline. Gray shaded region indicates the time window over which the transition rate is calculated. Baseline is defined slightly differently for the kernel-shaped stimuli compared to the triangle waves, see methods. Of 13,612 and 14,699 stimulus-animal presentations for Forward 4 and Forward 5 kernel-shaped stimuli, and 340,757 stimulus-animal presentations for the triangle wave, the following number of transitions were observed: 26, 24, 2,604, 2,634 for Forward 4→5 (top row) and 6, 7, 713, 791 for Forward 6→5 (bottom row). To test significant change from baseline a t-test was used and the following p-values were observed: $\{5.5 \cdot 10^{-5}, 6.9 \cdot 10^{-6}, 1.8 \cdot 10^{-19}, 5.1 \cdot 10^{-48}\}$ for Forward 4→5 (top row) and $\{6.3 \cdot 10^{-2}, 8.7 \cdot 10^{-1}, 3.9 \cdot 10^{-2}, 6.7 \cdot 10^{-5}\}$ for Forward 6→5 (bottom row). Error bars show the standard error of the mean.

by slowing down or speeding up in a relative way instead of transitioning to a stimulus-defined velocity. This is of interest because it implies a form of context dependency: it suggests that the same stimulus will drive the animal into forward locomotory states of different speeds depending on the animal's current state.

To validate whether the stereotyped speed-up or slow-down stimulus indeed causes the animal to speed up or slow-down, we again inspected the animal's response to the kernel-shaped stimulus or the triangle-wave stimulus. Indeed, we find that the same stimulus drives the animal into a different forward locomotory state depending on the animal's current state, see **Figure 7**. For example, animals in the slower Forward 4 state responded to a Forward 4 kernel-shaped stimulus by *decreasing* their transitions to Forward 5. In contrast animals in the faster Forward 6 state responded to the same stimulus by *increasing* their transitions into Forward 5. This was one of multiple instances where we observed the animal responding to the same stimuli with opposite responses depending on its current behavior. During triangle wave stimulation, for example, an increasing ramp causes slowing down, while a decreasing ramp causes speeding up, see **Figure 7**. We therefore conclude that stereotyped mechanosensory signals drive the animal to speed up or slow down.

Attention to mechanosensory signals depends on the animal's current behavior

When the animal turns it ignores all tested mechanosensory signals. This surprising observation is predicted by reverse-correlation analysis and confirmed by optogenetic and tap stimulation. Transitions out of Turn are uncorrelated with stimulus, and kernels for those transitions all fail to pass our shuffled significance threshold, see bottom row in **Figure 6** - Figure Supplement 1.

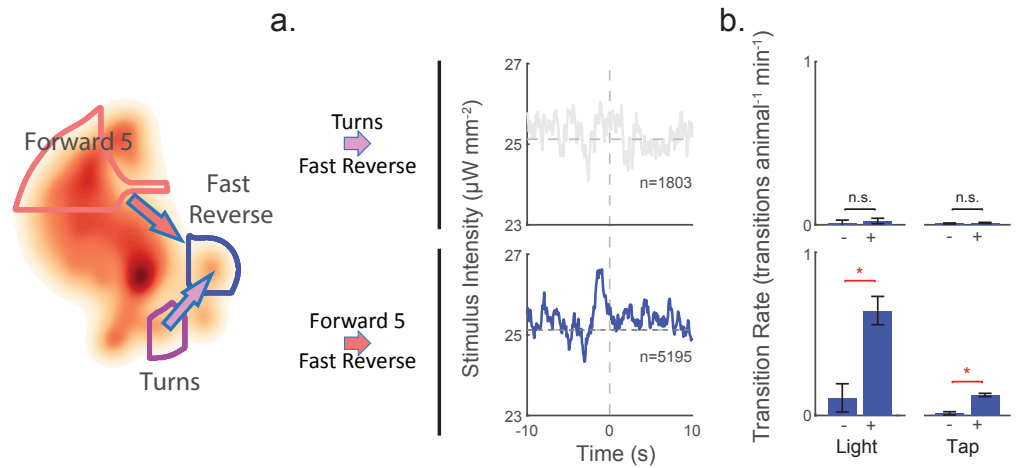


Figure 8. Attention to mechanosensory signals depends on behavior. When the animal is in the turn state it ignores mechanosensory stimuli. **a.)** Kernels are shown for two context-dependent transitions into Fast Reverse. Transitions into Fast Reverse originating from Forward 5 are correlated with stimulus and have a significant kernel while those originating from Turns are not and fail our shuffled significance threshold, see methods. Kernels shown are same as in *Figure 6* - Figure Supplement 1 **b.)** Transition rate in response to light and tap are shown. Animals in the turn state show no significant change in transition rates in response to light or tap, while animals in other states, like Forward 5 do. The 2 second post-stimulus mean transition rate into Fast Reverse is shown in response to a 1 s light stimulation (+), mechanical tap (+) or a mock control (-). Star indicates significance, calculated using an E-test, see methods. Error bars show standard error of the mean. 2,487 and 37,000 stimulus-animal presentations were analyzed for light(+) and tap(+) respectively, and 2,427 and 40,012 mock controls(-) for light and tap. The following number of transitions were observed {1, 2, 11, 15} for Turns→Fast Reverse (top row) and {9, 55, 18, 160} for Forward 5→Fast Reverse (bottom row). P-values for the E-test are {0.68, 0.34} for Turns→Fast Reverse (top row) and $\{1.96 \cdot 10^{-9}, 0\}$ for Forward 5→Fast Reverse (bottom row)

Figure 8-Figure supplement 1. Transition rates in response to light pulse for all pairwise transitions.

Figure 8-Figure supplement 2. P-values for transition rates in response to light pulse for all pairwise transitions.

Figure 8-Figure supplement 3. Transition rates in response to tap for all pairwise transitions.

Figure 8-Figure supplement 4. P-values for transition rates in response to tap for all pairwise transitions.

Consequently, the kernels predict that the animal should ignore mechanosensory stimuli during turns. In contrast, for every other behavior state there is always at least one (and often many) transitions exiting out of the state whose kernels pass our significance threshold (all rows other than Turn have at least one significant kernel).

To further test whether the animal indeed ignores stimuli during turns, we investigated the animal's context-dependent response to light pulses or tap. When the animal was in the Turn state, neither light pulse nor tap evoked a significant change in the rate of transitions into any other behavior, see bottom row **Figure 8** - Figure Supplement 1 and 3 (multiple-hypothesis corrected E-test, see methods). In contrast, when the animal was in other states like Forward 5, both tap and light pulses evoked significant changes in the transition rate into other behaviors. In fact, every other behavior state except for Forward 2 had at least one behavior transition exiting the state whose transition rate was significantly affected by either light or tap. The Turn behavior state alone was unique in that none of the kernels for transitions originating in Turn were significant, and no transition rates changed significantly in response to either light or tap. We therefore conclude that in Turn, but not other states, the animal ignores mechanosensory stimuli.

Transitions into Fast Reverse provide an illustrative example, see **Figure 8**. When the animal is in the Turn state, there is no significant difference in the rate of Turn→Fast Reverse transition between shuffled and stimuli. But when the animal is in Forward 5, light and taps caused a significant increase in Forward 5→Fast Reverse. Taken together, we conclude that the animal attends to mechanosensory signals during most behavior states, like Forward 5, but ignores it during Turns. In the discussion we explore why this may be ethologically relevant.

Discussion

This work revises a number of implicit assumptions about *C. elegans* sensory processing. First, the animal's behavioral response is not merely determined by the amplitude of signals in the touch neurons. Instead, it is also tuned to temporal properties of these signals, like the derivative, that extend over many seconds in time. Moreover, by adjusting a stimulus waveform, mechanosensory signals in the same neurons can be tailored to elicit different behavioral responses. Second, mechanosensory signals influence a broader set of behaviors than previously reported. Mechanosensation not only drives reversals and accelerations but it can also evoke the animal to slow down. Third, even short term behavior states can influence the animal's sensory processing. Earlier work has emphasized context-dependent sensory processing for behaviors with timescales of minutes to hours, like hunger-satiety (*Ghosh et al., 2016*), quiescence (*Schwarz et al., 2011; Nagy et al., 2014b*) and arousal (*Cho and Sternberg, 2014*). Here we show that even seconds-long timescale behaviors can dramatically alter how the animal responds to a stimulus. Most dramatically, when the animal turns it appears to ignore mechanosensory signals completely.

In more complex sensory systems like the retina, we have come to expect that the nervous system is carefully tuned to temporal properties of sensory signals (*Meister and Berry, 1999*). Recently it was shown that in drosophila, temporal processing is important for behavioral responses to odors, light and sound (*Behnia et al., 2014; Coen et al., 2014; Gepner et al., 2015; Hernandez-Nunez et al., 2015*). And in the much simpler *C. elegans*, temporal processing on order second timescale has been observed in thermosensation (*Clark et al., 2006, 2007*), and chemosensation (*Kato et al., 2014*) where it is known to be crucial for guiding thermotaxis or chemotaxis. In the *C. elegans* mechanosensory circuit, it had been known that temporal processing occurs at the receptor level to convert applied forces into evoked currents on the tens of milliseconds timescale (*Eastwood et al. (2015)*), but it had remained unclear whether the nervous system used temporal information downstream for determining the animal's behavioral response. In this work we now see evidence of temporal processing on behavior-relevant timescales that guides the animal's behavioral response. That such behavior-relevant temporal processing is observed even in the simple mechanosensory circuit raises the possibility that temporal processing may be ubiquitous across sensory systems for driving behavior. Why might it be beneficial for the *C. elegans* nervous

Table 1. Forward and reverse primer sequences used to generate pAL::p*mec-4*::*Chrimson*::*SL2*::*mCherry*::*unc-54*.

Primer	Sequence
mec-4_fwd	AAGCTTCAATACAAGCTC
mec-4_rev	TAAGTTGATAGCGATAAAAAAATAG
CHRIMSON_fwd	ATGGCTGAGCTTATTCATC
CHRIMSON_rev	AACAGTATCTTCATCTTCC
SL2_fwd	GGTACCGCTGTCTCATCC
SL2_rev	GATGCGTTGAAGCAGTTTC
mCherry_fwd	ATGGTCTCAAAGGGTGAAG
mCherry_rev	TTATAACAATTCATCCATGCC
U54_fwd	GCGCCGGTCTGCTACCATTAC
U54_rev	AAGGGCCCGTACGGCCGA

system to have evolved to tune its behavioral response to temporal properties of mechanosensory signals, like the derivative, over seconds? We speculate that perhaps it is important for the worm to react differently if mechanosensory signals are increasing or decreasing, rather than merely base its decision on the overall strength.

That the animal ignores mechanosensory inputs during turning is striking and surprising. Why might the animal have evolved to ignore such signals during turns? The turn is part of the *C. elegans* escape response, an avoidance behavior with similarities to escape responses in other organisms like crayfish, mullusks or goldfish (Pirri and Alkema, 2012). *C. elegans* escape consists of reverse locomotion, followed by a turn and then forward locomotion in a new direction. The turn allows the animal to reorient and navigate away from a predator, and defects in this circuit have been shown to decrease survivability (Maguire et al., 2011). Failing to complete the turn could inadvertently cause the animal to retrace its steps and return to danger.

Ultimately we see evidence of two kinds of internal processes that govern how the animal interprets sensory signals. First the animal integrates mechanosensory information over seconds timescale. Second, the animal interprets these signals differently depending on the animal's behavior state. An exciting future direction will be to identify the neural circuit mechanisms which allows the worm's nervous system to integrate mechanosensory signals over time; and to rapidly alter its response to mechanosensory signals depending on behavior state. This could shed insight into how internal brain states rapidly modulate sensory processing in a simple model system.

Methods and Materials

Strains

The two strains used in this study were wild-type N2 Bristol animals; and AML67 (wtf1s46[p*mec-4*::*Chrimson*::*SL2*::*mCherry*::*unc-54*]), a transgenic strain that expresses the light-gated ion channel *Chrimson* and a fluorescent protein *mCherry* in mechanosensory neurons. To generate AML67, 40 ng of plasmid (pAL::p*mec-4*::*Chrimson*::*SL2*::*mCherry*::*unc-54*) were injected into N2 animals, integrated via UV irradiation (Evans, 2006), and outcrossed with N2 six times. AML67 has been deposited in the public *Caenorhabditis* Genome Center repository. Plasmid pAL::p*mec-4*::*Chrimson*::*SL2*::*mCherry*::*unc-54* (<https://www.addgene.org/107745/>) was engineered using HiFi Cloning Kit (NEB). *Chrimson* was a kind gift of Boyden Lab. *mCherry* and backbone was amplified from pJIM20, gift from John Murray, U Penn. Promoter sequence (*mec-4*), splicing sequence (*SL2*) and 3'-utr sequence (*unc-54*) were amplified using primers as listed in Table 1. Construct was sequenced confirmed before injection.

Transgenic animals exhibited reduced sensitivity to tap or touch compared to wild-type, presumably because *Chrimson* competes with endogenous MEC-4 protein for transcription, see Figure 2 -

Figure Supplement 4. From the alleles we had generated, we selected AML67 for use in this study because it was the most sensitive to tap and touch, despite being reduced compared to wild-type.

Nematode handling

Strains were maintained on 9 cm NGM agar plates seeded with OP50 *E. coli* food, at 20 °C. Worms were bleached 3 days prior to experiment to provide 1 day old adults. For optogenetic experiments, bleached worms were placed on plates seeded with 1 mL of 0.5 mM all-trans-retinal (ATR) mixed with OP50. Control plate lacked ATR. To avoid inadvertent optogenetic activation, plates were wrapped in aluminum foil, handled in the dark, and viewed under dissection microscopes using dim blue light.

To harvest worms for high-throughput experiments, roughly 100 to 200 worms were cut from agar and washed and then spun-down in a 1.5 mL microcentrifuge tube. Worms at the bottom of the tube were placed on an unseeded 9 cm NGM agar plate via micropipette. Excess liquid on the plate was carefully wicked away using tissue paper. Worms were allowed to adapt to their new environment for 25 minutes before recordings or stimulation.

High-throughput imaging

Experiments were conducted in a custom-built high-throughput imaging rig (*Figure 2* - Figure Supplement 1). Plates of animals were recorded while undergoing 30 minutes of optogenetic or tap stimulation. Imaging was performed as follows: The agar plate was illuminated by a ring of 850 nm infrared LEDs (irrf850-5050-60-reel, environmentallights.com). A 2,592 x 1,944 pixel CMOS camera (ACA2500-14um, Basler) recorded worm movements at 14 frames per second and a magnification of 20 μm per pixel so as to provide sufficient spatiotemporal resolution to capture posture dynamics. The field of view of the camera was centered on the plate and included approximately 50% of plate surface. Custom LabVIEW software acquired images from the camera and controlled stimulus delivery as described below.

Tap delivery

Taps were delivered to the side of 9 cm plates containing the animals by means of a solenoid, similar to (*Swierczek et al., 2011*). An electric solenoid tapper (Small Push-Pull Solenoid, Adafruit) was driven with a 70 ms, 24 V, DC pulse under Labview control via a LabJack DAQ and a solid-state relay. During tap experiments, taps were delivered to the plate once per minute for 30 minutes, see *Table 2*. The 1 minute inter-stimulus interval was chosen to minimize habituation (*Timbers et al., 2013*).

Optogenetic stimulation

Experiments involving optogenetic stimulation are summarized in *Table 2*. Optogenetic stimulation was delivered by three 625 nm LEDs (M625L3, Thorlabs) positioned such that their light approximately tiles the agar plate visible in the camera's field of view. LED's were driven by a diode driver (L2C210C, Thorlabs) under the control of LabVIEW via an analog signal from a LabJack DAQ (Model U3-HV with LJTick-DAC). The range of the light intensity for optogenetic stimulation averaged at the plate spanned from 0 to 80 $\mu\text{W mm}^{-2}$. Small spatial inhomogeneities in light intensity were characterized and accounted for in software so as to calculate the precise light intensity delivered to each animal. A infrared long pass filter (FEL0800, Thorlabs) in front of the camera blocked light from the stimulus LEDs and only permitted light from the infrared behavior LEDs.

Optogenetic pulse stimulus

For optogenetic pulse experiments, as in *Figure 2*, a 1 second light pulses was delivered once per minute for 30 minutes. Initial experiments measured the behavioral responses to pulses of different light intensities. In those experiments, shown in *Figure 2c*, the light intensity of the pulse

was randomly shuffled such that five pulses each of 2, 5, 10, 50, and 80 $\mu\text{W mm}^{-2}$ were delivered during the 30 minute recording.

Random noise optogenetic stimulus

Experiments involving reverse correlation all used a light stimulus with intensity modulated by random broad-spectrum noise. The random noise stimulus was generated according to,

$$s(t + 1) = As(t) + Bn_{\text{rand}} + C, \quad (2)$$

where $A \equiv \exp(-\tau_{\text{period}}/\tau_c)$ and $B \equiv \sigma_{\text{rms}} \sqrt{1 - A^2}$. Here $s(t + 1)$ is the stimulus intensity at the next time-point, A is the weighting of the previous stimulus $s(t)$, B is the weighting of a random number, n_{rand} , drawn from a Gaussian distribution with standard deviation given by σ_{rms} , and C is a constant offset that sets the average stimulus intensity. The weighting A is related to correlation time τ_c and the duration of our time step τ_{period} . Because in our setup the stimulus is updated with each image acquisition, the time step τ_{period} is the inverse of the image acquisition rate, or approximately 0.07 s for 14 Hz.

Both C and σ_{rms} were chosen to be 25 $\mu\text{W mm}^{-2}$ so that the the function generated intensities that mostly fell in the intensity range of 0 to 50 $\mu\text{W mm}^{-2}$, a regime that appeared to be most sensitive to behavior response (see [Figure 2c](#);). τ_c was chosen to be 0.5 s as this roughly matched our intuition about the timescale of temporally varying mechanical stimuli that the animal might encounter while navigating its natural environment. Finally, the stimulus was clipped and forced to stay in the range of 0 to 50 $\mu\text{W mm}^{-2}$. Frequency spectra of our stimuli is shown in [Figure 3](#) - Figure Supplement 4.

Triangle wave optogenetic stimulus

Triangle wave stimuli were also generated. Triangle waves were linearly increasing ramps of light intensity from 0 $\mu\text{W mm}^{-2}$ to 50 $\mu\text{W mm}^{-2}$ for 10 seconds followed by linearly decreasing ramps 50 $\mu\text{W mm}^{-2}$ to 0 $\mu\text{W mm}^{-2}$ for 10 seconds, repeated continuously for 30 minutes.

Kernel-shaped (tailored) stimulus

In the tailored stimulation experiments, stimuli were generated from the behavior triggered averages found using reverse correlation. The six behavior triggered averages from [Figure 3](#) were scaled in intensity until either their minimum was at 0 $\mu\text{W mm}^{-2}$ or the maximum was at 50 $\mu\text{W mm}^{-2}$. These were then shuffled and played back one per minute such that each behavior triggered averages was delivered 5 times per 30 minute experiment. 25 $\mu\text{W mm}^{-2}$ of constant light intensity was delivered between stimulus presentation.

Table 2. Summary of experimental conditions. Each experimental series consisted of recordings of multiple plates usually spread across multiple days, as indicated. Recordings were all 30 mins in duration per plate. Note two methods were used to tally the number of stimulus-animal presentations (see methods). Here a stimulus presentation is counted even if the track was interrupted mid-presentation.

Experiment Series	Strain	Stim	ATR	# of Plates	# of Days	Interstim Interval (s)	Stimulus Duration (s)	Total Animal-Stimulus Presentations	Cumulative Recording Length (animal-hours)	Animals per frame (Mean±Stdev)	Figures
Random Noise	AML67	Light	+	58	3	n/a	n/a	n/a	1,784	62±34	<i>Figure 1, Figure 1-Supp 2, Figure 1-Supp 3, Figure 1-Supp 4, Figure 3, Figure 3-Supp 1, Figure 3-Supp 2, Figure 3-Supp 4, Figure 6, Figure 6-Supp 1, Figure 8</i>
			-	20	3	n/a	n/a	n/a	500	50±23	<i>Figure 1, Figure 1-Supp 2, Figure 1-Supp 3, Figure 3-Supp 1, Figure 3-Supp 3, Figure 6-Supp 2</i>
Triangle Wave	AML67	Light	+	62	3	0	20	340,757	1,912	62±42	<i>Figure 5, Figure 7</i>
			-	20	3	0	20	142,461	800	80±55	<i>Figure 5-Supp 1</i>
Kernel-Shaped Stimuli	AML67	Light	+	44	3	40	20	84,875	1,453	66±40	<i>Figure 4, Figure 4-Supp 1, Figure 7</i>
			-	12	3	40	20	22,866	392	65±33	<i>Figure 4-Supp 2</i>
Light Pulse	AML67	Light	+	12	1	59	1	15,128	260	43±24	<i>Figure 2, Figure 8</i>
			-	6	1	59	1	8,107	139	46±18	<i>Figure 2-Supp 3</i>
Plate Tap	AML67	Tap	+	7	2	60	Impulse	21,117	366	105±60	<i>Figure 2-Supp 4</i>
			-	8	2	60	Impulse	14,646	254	64±46	
	N2	Tap	-	22	3	60	Impulse	40,409	695	63±25	<i>Figure 2, Figure 8, Figure 8-Supp 3</i>
Total				271					8,554	63±40	

Measuring animal behavior

The unsupervised behavior mapping approach used in this work is adapted from the fly (*Berman et al., 2014*) and is similar in spirit to work in rodents (*Wiltschko et al., 2015*). It also builds upon decades of methodological advances quantifying *C. elegans* behavior (*Croll, 1975a,b; Stephens et al., 2008; Ramot et al., 2008; Brown et al., 2013; Yemini et al., 2013; Gyenes and Brown, 2016; Gomez-Marin et al., 2016*).

Animal behavior was measured and classified using an analysis pipeline, summarized in *Figure 1* - Figure Supplement 1. First, worms were located and tracked, then their posture was extracted, and finally their posture dynamics were clustered and classified. Details of the pipeline are described below. The pipeline was written in MATLAB and run on the Princeton University's high performance parallel computing cluster. Source code is available at (<https://github.com/leiferlab/liu-temporal-processing>).

Animal location tracking

To first identify animals and track their location, raw video of animals on plates were analyzed using a modified version of the Parallel Worm Tracker (*Ramot et al., 2008*). Animal's were found via binary thresholding and centroid tracking.

Animal posture extraction

The animal's posture was found by extracting the animal's centerline from the video using custom MATLAB scripts. Videos of each individual worm were first generated by cropping a 70x70 pixel region around the worm's centroid at every frame. A centerline with 20 points was fitted to the image at each frame using an active contour model similar to (*Nguyen et al., 2017*), inspired by the one described by (*Deng et al., 2013*). The algorithm for fitting the centerline was specifically optimized to measure posture of the worm in a variety of conditions, including when the animal crossed over itself during turns. The active contour model fits the centerline by relaxing contiguous points along a gradient defined by four forces: (1) an image force that fit the contour to the image of the worm; (2) a tip force that guides the beginning and end of the contour to the worm's presumptive head and tail; (3) a spring force that guides the contour to be similar lengths; (4) and a repel force that makes sure that the contour does not stick to itself. To ensure continuity in time, the active contour of the following frame is initialized by the relaxed contour of the previous frame. The head and the tail of the worm was determined by assuming the worm moves forward the majority of the time. A quality score was calculated to estimate how well the centerline fit the image and how much it displaced from the previous centerline. On the rare occasion when the quality score of a frame fell below threshold, that frame was dropped, and the track was split into two.

Posture dimensionality reduction

To more efficiently interpret the animal's posture, the dimensionality of the animal's centerline was reduced from 20 position (x, y) coordinate to five posture coefficients using principle component analysis (PCA), following (*Stephens et al., 2008*). Principle components of posture were extracted from recordings of approximately 2 million animal-frames of freely behaving N2 worms. Centerlines were converted into a series of angles oriented such that the mean angle is 0. The first five principle components explain >98% of the posture variance. The animal's posture dynamics were thus represented as a time-series of five coefficients, one for each of the five principle posture modes.

Generating spectrograms of posture dynamics

To characterize posture dynamics, a spectrogram was generated for each of the posture mode coefficients, as in (*Berman et al., 2014*). A Morlet continuous wavelet transform was performed on each of the 5 coefficient time series at 25 frequencies dyadically spaced between 0.3 Hz and 7 Hz. The low frequency bound was chosen to reflect our intuition regarding the timescale of *C. elegans* behavior and the high frequency bound was set by the Nyquist sampling frequency of

our image acquisition. The spectrogram provides information about the frequency spectra of the animal's posture dynamics but it lacks information about the phase of the animal's posture, which is important for discerning forward from backward locomotion. To preserve forward and backward information, we introduced a binary "directionality" vector that is 2 when the worm centroid is moving forward, and 1 when the worm centroid is backwards. Directionality was calculated by taking the sign of the dot product of the head vector with a tangent vector of the animal's centroid trajectory. Together, the five spectrograms and directionality vector provide a 126 dimensional feature vector that describe the animal's behavior at each time point. It is this feature vector that is clustered, as described below.

Defining the behavioral map and behavior states

To classify behavior into discrete stereotyped behavior states that emerge naturally from our recordings, we followed a behavior-mapping strategy described in (Berman *et al.*, 2014). A single behavior map was generated so that behaviors were defined consistently across all experiments. To generate the behavior map, 50,000 animal-time points were uniformly sampled from the 2,284 animal-hours of behavior recordings made during random-noise optogenetic stimulation. Each animal-time point contributes a 126-dimensional feature vector describing the animal's instantaneous behavior. We generated a 2D map of these feature vectors by embedding the 126 dimensional space in a plane using non-linear dimensionality reduction technique called t-distributed stochastic neighbor embedding (t-SNE) (Maaten and Hinton, 2008). Under t-SNE, each feature vector is embedded such that the local distance between feature vectors is conserved but long distance scales are distorted (Figure 2 - Figure Supplement 2a).

We then generated a probability density histogram of behavior by projecting all 10^8 behavior time points from the 2,284 animal-hours of random noise optogenetic stimulation (Figure 1 - Figure Supplement 2b) into the 2D map. Clusters of high probability in this density map corresponded to a distinct stereotyped behavior. Stereotype behaviors were defined by water-shedding the probability density map (Figure 1 - Figure Supplement 2c) and each region was assigned a name like "Forward 3" (Figure 1b). Examples of worms in each region are shown in Figure 1 - Figure Supplement 3. Time points from subsequent recordings were similarly projected into this map for the purposes of classifying animal behavior.

Identifying behavioral transitions

At each time point, the worm belongs to a point in the 2D behavior map described above (see Figure 1 - Figure Supplement 4). Animals that dwelled in one behavior region for at least 0.5 seconds were classified as exhibiting that behavior during all contiguous time points in that behavior region. Animal's inhabiting a behavior region for less than 0.5 seconds were classified as "in transition."

A "transition into behavior X " is defined to occur on the first time point that the animal is classified as in X . Transitions from behavior $W \rightarrow X$ were defined to occur on the first time point the animal is classified as in X provided that: the animal transitioned directly from W to X ; or the animal had previously been classified as in W , was then classified as "in transition" and then was classified as in state X . Cases where the animal was in X , then "in transition" and then returned to X , were ignored.

Ambiguities in temporal definition of behavior

The wavelet spectrogram introduces an inherent uncertainty in the precise timing of a behavior transition. This ultimately arises from the uncertainty principle: behavior dynamics that have low frequency components provide less temporal resolution than higher frequency dynamics. An equivalent view is that the spectrogram feature vector at any given moment is influenced by temporally adjacent postural dynamics in the past and future, and this influence is stronger at lower frequencies than higher ones.

This temporal uncertainty or "bleeding over" of future behavior, causes the animal occasionally

to appear to (but not actually to) respond to a stimulus prior to its delivery. In the worst case, the time-scale of this leakage is set by our choice of the lowest frequency wavelet, which is 0.3 Hz (i.e. 2.7 seconds). Behaviors with strong higher-frequency components have shorter timescale uncertainties. We take large time windows of 20 seconds to define our kernels, in part, so that a few second time-shift does not result in any loss of information.

Reverse correlation

Reverse correlation was used to find a linear kernel and non-linearity that describe the relationship between the animal's behavior transitions and an applied stimulus.

Calculating kernels

Linear kernels for each behavior were estimated by computing the behavior-triggered-average of the stimulus,

$$\hat{A} = \frac{1}{N} \sum_{n=1}^N \vec{s}(t_n), \quad (3)$$

where t_n is the time of n th behavioral transition, $\vec{s}(t_n)$ is a vector representing the stimuli presented during a 20 second temporal window around t_n and N is the total number of behavioral transitions (*Schwartz et al., 2006*). The linear kernel was estimated to be the mean-subtracted, time-reversed behavior-triggered average.

Kernel significance

Behavior triggered averages (also referred to as kernels) were deemed significant if their magnitude (L2 norm) exceeded the top 1 percent of a distribution of random kernels found by shuffling the stimulus in time. Shuffling was performed in such a way as to preserve the temporal properties of the transition train while completely decorrelating it from the stimulus. Specifically, shuffling was performed by circle-shifting the transition timings within every track by a randomly selected integer between 1 and the number of time points in the track. Shuffled kernel distributions for each behavior were generated by recalculating the behavior triggered-average 100 times, each with different circle-shifted timings.

Estimating the non-linearity

The non-linearity f allows the probability of a behavior transition to be estimated from the filtered signal namely the stimulus convolved with the linear kernel (*Gepner et al., 2015*). Non-linearities were estimated from the ratio of two histograms: the first is a histogram of time-point counts versus filtered signal given a behavioral transition at that time-point, and the second is a histogram of time-point counts versus filtered signal for all time-points (*Schwartz et al., 2006*). Histograms were tabulated with 10 equally spaced bins spanning the range of the filtered signal. Bin-wise division of the two histograms yielded 10 points relating probability of behavior to filtered signals (*Figure 3 - Figure Supplement 2*). For each point, we calculate a propagated error, E , assuming Poisson counting statistics,

$$E = \sqrt{\frac{T-1}{F^2} + \frac{T^2(F-1)}{F^4}}, \quad (4)$$

where T is the number of behavioral transitions in that bin, and F is the number of filtered signal time-points in that bin. We then fitted a 2 parameter exponential to the 10 points, weighing each point by the inverse of the error in order to reduce the influence of noise. This fitted exponential function is our estimate of the non-linearity.

Calculating transition rates

When presented as a timeseries of rates, as in *Figure 2 - Figure Supplement 2*, transition rates were calculated according to the following: Behavior timeseries from all recordings were cropped in a time window around each stimulus, commingled, and then time aligned to the stimulus. The

fraction of all animals undergoing a transition was calculated at each time step. The fractions of animal were directly converted into a rate of transitions per animal per minute, yielding the timeseries of rates.

Calculating transition rate changes

Transition rate change, as in *Figure 4b*, *Figure 4* - Figure Supplement 1, *Figure 5*, and *Figure 7*, were calculated as follows: an average transition rate was found in a time window during a stimulus (as described above), and then a baseline was subtracted off. For kernel-shaped stimuli experiments (*Figure 4a* and *Figure 4* - Figure Supplement 1) the baseline is defined as the average transition rate in a 20 second time window prior to each stimulus. For the triangle wave in *Figure 5*, the baseline was defined to be the overall mean transition rate throughout the recording.

In cases where a bar is shown (*Figure 4a*, *Figure 7*), a change in transition rate was calculated by averaging the timeseries of rates over a time window (indicated in figures with gray shading).

Measuring transition rates for tap or light induced context dependent transitions

Transition rates were calculated slightly differently in *Figure 8* and *Figure 8* - Figure Supplement 1 and 3 to facilitate significance testing via the E-test *Krishnamoorthy and Thomson (2004)*. The transition rate in a two second time window immediately following light pulse or tap (+) was compared to a transition rate in a two second window immediately following a mock control (-). Mock controls were set to occur at the mid point between consecutive stimuli.

Instead of calculating the transition rates at each time bin and then averaging across time, as described previously, we instead calculated a single transition rate for the entire two second time window by comingling transitions from all time bins, as follows. We 1) selected tracks that were uninterrupted for the 2 seconds, (2) counted the total number of given transition in the 2 seconds after stimulus onset across all of our experiments, (3) divided by the total number of tracked time points, and (4) converted the value to transitions per animal per minute. The number of stimulus-animal presentations differs slightly from those in *Figure 2* because now tracks are required to be contiguous for 2 seconds after stimulus presentation, which was not a requirement previously.

P-values were attained using an E-test (*Krishnamoorthy and Thomson, 2004*). To account for testing 72 behavior transitions concurrently, we use the Bonferroni multiple-hypothesis correction. Only p-values less than $\alpha = 0.05/72 = 7 \cdot 10^{-1}$ are considered significant.

In our analysis of light pulse response, we grouped all stimulation light intensities together.

Data

Behavioral analysis and stimulation data for all tracked animals in all experiments in *Table 2* are available at <https://doi.org/10.6084/m9.figshare.5956348>. See dataset README for details. All recorded data, including raw images (>1 TB), are being made available at <http://dx.doi.org/10.21227/H27944>.

Acknowledgments

We thank Marc Gershow (NYU) and Gordon Berman (Emory) for productive discussions and troubleshooting. We also thank Mala Murthy and Jonathan Pillow, both of Princeton University, for productive discussions and feedback. Alicia Castillo Bahena and Tayla Duarte contributed to preliminary studies of this work.

Wild type N2-type strains were procured from Caenorhabditis Genetic Center (CGC), Minnesota.

This work was supported by grants from the Simons Foundation (SCGB #324285, and SCGB #543003, A.M.L.). This work was also supported by Princeton University's Dean for Research Innovation Fund to A.M.L. and J.W.S. Research reported in this publication was supported by the National Human Genome Research Institute of the National Institutes of Health under Award

Number T32HG003284. The content is solely the responsibility of the authors and does not necessarily represent the official views of the National Institutes of Health.

Author Contributions

M.L. conducted all experiments and analysis. A.K.S. performed all transgenics. A.M.L., J.W.S. and M.L. conceived all experiments. All authors reviewed and edited the manuscript.

References

- Ardiel EL**, Yu AJ, Giles AC, Rankin CH. Habituation as an adaptive shift in response strategy mediated by neuropeptides. *npj Science of Learning*. 2017 Aug; 2(1):9. <https://www.nature.com/articles/s41539-017-0011-8>, doi: 10.1038/s41539-017-0011-8.
- Behnia R**, Clark DA, Carter AG, Clandinin TR, Desplan C. Processing properties of ON and OFF pathways for *Drosophila* motion detection. *Nature*. 2014 Aug; 512(7515):427–430. <https://www.nature.com/articles/nature13427>, doi: 10.1038/nature13427.
- Berman GJ**, Choi DM, Bialek W, Shaevitz JW. Mapping the stereotyped behaviour of freely moving fruit flies. *Journal of the Royal Society, Interface / the Royal Society*. 2014 Oct; 11(99). doi: 10.1098/rsif.2014.0672.
- Brown AEX**, Yemini EI, Grundy LJ, Jucikas T, Schafer WR. A dictionary of behavioral motifs reveals clusters of genes affecting *Caenorhabditis elegans* locomotion. *Proceedings of the National Academy of Sciences of the United States of America*. 2013 Jan; 110(2):791–796. doi: 10.1073/pnas.1211447110.
- Calhoun AJ**, Murthy M. Quantifying behavior to solve sensorimotor transformations: advances from worms and flies. *Current Opinion in Neurobiology*. 2017 Oct; 46:90–98. <http://www.sciencedirect.com/science/article/pii/S095943881730123X>, doi: 10.1016/j.conb.2017.08.006.
- Chalfie M**, Sulston JE, White JG, Southgate E, Thomson JN, Brenner S. The neural circuit for touch sensitivity in *Caenorhabditis elegans*. *The Journal of Neuroscience: The Official Journal of the Society for Neuroscience*. 1985 Apr; 5(4):956–964.
- Chalfie M**, Sulston J. Developmental genetics of the mechanosensory neurons of *Caenorhabditis elegans*. *Developmental Biology*. 1981 Mar; 82(2):358–370. <http://www.sciencedirect.com/science/article/pii/0012160681904590>, doi: 10.1016/0012-1606(81)90459-0.
- Chiba CM**, Rankin CH. A developmental analysis of spontaneous and reflexive reversals in the nematode *Caenorhabditis elegans*. *Journal of Neurobiology*. 1990 Jun; 21(4):543–554. doi: 10.1002/neu.480210403.
- Cho J**, Sternberg P. Multilevel Modulation of a Sensory Motor Circuit during *C. elegans* Sleep and Arousal. *Cell*. 2014 Jan; 156(1):249–260. <http://www.sciencedirect.com/science/article/pii/S0092867413015201>, doi: 10.1016/j.cell.2013.11.036.
- Clark DA**, Biron D, Sengupta P, Samuel ADT. The AFD sensory neurons encode multiple functions underlying thermotactic behavior in *Caenorhabditis elegans*. *The Journal of Neuroscience: The Official Journal of the Society for Neuroscience*. 2006 Jul; 26(28):7444–7451. <http://www.ncbi.nlm.nih.gov/pubmed/16837592>, doi: 10.1523/JNEUROSCI.1137-06.2006.
- Clark DA**, Gabel CV, Gabel H, Samuel ADT. Temporal Activity Patterns in Thermosensory Neurons of Freely Moving *Caenorhabditis elegans* Encode Spatial Thermal Gradients. *J Neurosci*. 2007 Jun; 27(23):6083–6090. <http://www.jneurosci.org/cgi/content/abstract/27/23/6083>, doi: 10.1523/JNEUROSCI.1032-07.2007.
- Clemens J**, Murthy M. The Use of Computational Modeling to Link Sensory Processing with Behavior in *Drosophila*. In: *Decoding Neural Circuit Structure and Function* Springer, Cham; 2017.p. 241–260. https://link.springer.com/chapter/10.1007/978-3-319-57363-2_9, doi: 10.1007/978-3-319-57363-2_9.
- Coen P**, Clemens J, Weinstein AJ, Pacheco DA, Deng Y, Murthy M. Dynamic sensory cues shape song structure in *Drosophila*. *Nature*. 2014 Mar; 507(7491):233–237. <https://www.nature.com/articles/nature13131>, doi: 10.1038/nature13131.
- Croll N**. Behavioural analysis of nematode movement. *Advances in Parasitology*. 1975; 13:71–122.

- Croll N.** Components and patterns in the behavior of the nematode *Caenorhabditis elegans*. *Journal of Zoology*. 1975; 176:159–176. <http://www.wormbase.org/db/misc/biblio?name=BEHAV%2FMOVEMENT&category=&class=Keyword&abstract=WBPaper00000075#WBPaper00000075>.
- Deng Y, Coen P, Sun M, Shaeviz JW.** Efficient Multiple Object Tracking Using Mutually Repulsive Active Membranes. *PLoS ONE*. 2013 Jun; 8(6):e65769. <http://dx.doi.org/10.1371/journal.pone.0065769>, doi: 10.1371/journal.pone.0065769.
- Driscoll M, Kaplan J.** Mechanotransduction. In: Riddle DL, Blumenthal T, Meyer BJ, Priess JR, editors. *C. elegans II*, 2nd ed. Cold Spring Harbor (NY): Cold Spring Harbor Laboratory Press; 1997.<http://www.ncbi.nlm.nih.gov/books/NBK20177/>.
- Eastwood AL, Sanzeni A, Petzold BC, Park SJ, Vergassola M, Pruitt BL, Goodman MB.** Tissue mechanics govern the rapidly adapting and symmetrical response to touch. *Proceedings of the National Academy of Sciences*. 2015 Dec; 112(50):E6955–E6963. <http://www.pnas.org/content/112/50/E6955>, doi: 10.1073/pnas.1514138112.
- Evans T.** Transformation and microinjection. *WormBook*. 2006; http://www.wormbook.org/chapters/www_transformationmicroinjection/transformationmicroinjection.html, doi: 10.1895/wormbook.1.108.1.
- Gepner R, Skanata MM, Bernat NM, Kaplow M, Gershow M.** Computations underlying *Drosophila* photo-taxis, odor-taxis, and multi-sensory integration. *eLife*. 2015 May; 4:e06229. <https://elifesciences.org/content/4/e06229v2>, doi: 10.7554/eLife.06229.
- Ghosh DD, Sanders T, Hong S, McCurdy LY, Chase DL, Cohen N, Koelle MR, Nitabach MN.** Neural Architecture of Hunger-Dependent Multisensory Decision Making in *C. elegans*. *Neuron*. 2016 Dec; 92(5):1049–1062. doi: 10.1016/j.neuron.2016.10.030.
- Gomez-Marin A, Stephens GJ, Brown AEX.** Hierarchical compression of *Caenorhabditis elegans* locomotion reveals phenotypic differences in the organization of behaviour. *Journal of The Royal Society Interface*. 2016 Aug; 13(121):20160466. <http://rsif.royalsocietypublishing.org/content/13/121/20160466>, doi: 10.1098/rsif.2016.0466.
- Gyenes B, Brown AEX.** Deriving Shape-Based Features for *C. elegans* Locomotion Using Dimensionality Reduction Methods. *Frontiers in Behavioral Neuroscience*. 2016; 10. <https://www.frontiersin.org/articles/10.3389/fnbeh.2016.00159/full>, doi: 10.3389/fnbeh.2016.00159.
- Hernandez-Nunez L, Belina J, Klein M, Si G, Claus L, Carlson JR, Samuel AD.** Reverse-correlation analysis of navigation dynamics in *Drosophila* larva using optogenetics. *eLife*. 2015 May; 4. doi: 10.7554/eLife.06225.
- Kato S, Xu Y, Cho CE, Abbott LF, Bargmann CI.** Temporal Responses of *C. elegans* Chemosensory Neurons Are Preserved in Behavioral Dynamics. *Neuron*. 2014 Feb; 81(3):616–628. [http://www.cell.com/neuron/abstract/S0896-6273\(13\)01088-X](http://www.cell.com/neuron/abstract/S0896-6273(13)01088-X), doi: 10.1016/j.neuron.2013.11.020.
- Kindt KS, Quast KB, Giles AC, De S, Hendrey D, Nicastro I, Rankin C, Schafer WR.** Dopamine Mediates Context-Dependent Modulation of Sensory Plasticity in *C. elegans*. *Neuron*. 2007 Aug; 55(4):662–676. <http://www.sciencedirect.com/science/article/pii/S0896627307005442>, doi: 10.1016/j.neuron.2007.07.023.
- Kitamura Ki, Amano S, Hosono R.** Contribution of neurons to habituation to mechanical stimulation in *Caenorhabditis elegans*. *Journal of Neurobiology*. 2001 Jan; 46(1):29–40. [http://onlinelibrary.wiley.com/doi/10.1002/1097-4695\(200101\)46:1<29::AID-NEU3>3.0.CO;2-8/abstract](http://onlinelibrary.wiley.com/doi/10.1002/1097-4695(200101)46:1<29::AID-NEU3>3.0.CO;2-8/abstract), doi: 10.1002/1097-4695(200101)46:1<29::AID-NEU3>3.0.CO;2-8.
- Krishnamoorthy K, Thomson J.** A more powerful test for comparing two Poisson means. *Journal of Statistical Planning and Inference*. 2004 Jan; 119(1):23–35. <http://www.ucs.louisiana.edu/~kxk4695/JSPI-04.pdf>, doi: 10.1016/S0378-3758(02)00408-1.
- Leifer AM, Fang-Yen C, Gershow M, Alkema MJ, Samuel ADT.** Optogenetic manipulation of neural activity in freely moving *Caenorhabditis elegans*. *Nature Methods*. 2011 Feb; 8(2):147–152. <http://www.ncbi.nlm.nih.gov/pubmed/21240279>, doi: 10.1038/nmeth.1554.
- Maaten Lvd, Hinton G.** Visualizing Data using t-SNE. *Journal of Machine Learning Research*. 2008; 9(Nov):2579–2605. <http://jmlr.org/papers/v9/vandermaaten08a.html>.
- Mazzochette EA, Nekimken AL, Loizeau F, Whitworth J, Huynh B, Goodman MB, Pruitt BL.** The Tactile Receptive Fields of Freely Moving *Caenorhabditis elegans* Nematodes. *bioRxiv*. 2018 Mar; p. 259937. <https://www.biorxiv.org/content/early/2018/03/05/259937>, doi: 10.1101/259937.

- Maguire S**, Clark C, Nunnari J, Pirri J, Alkema M. The *C. elegans* Touch Response Facilitates Escape from Predacious Fungi. *Current Biology*. 2011 Aug; 21(15):1326–1330. <http://www.sciencedirect.com/science/article/pii/S096098221100769X>, doi: 10.1016/j.cub.2011.06.063.
- Meister M**, Berry MJ. The neural code of the retina. *Neuron*. 1999 Mar; 22(3):435–450.
- Nagel G**, Brauner M, Liewald JF, Adeishvili N, Bamberg E, Gottschalk A. Light Activation of Channelrhodopsin-2 in Excitable Cells of *Caenorhabditis elegans* Triggers Rapid Behavioral Responses. *Current Biology*. 2005 Dec; 15(24):2279–2284. [http://www.cell.com/current-biology/abstract/S0960-9822\(05\)01407-7](http://www.cell.com/current-biology/abstract/S0960-9822(05)01407-7), doi: 10.1016/j.cub.2005.11.032.
- Nagy S**, Raizen DM, Biron D. Measurements of behavioral quiescence in *Caenorhabditis elegans*. *Methods*. 2014 Aug; 68(3):500–507. <http://www.sciencedirect.com/science/article/pii/S1046202314001029>, doi: 10.1016/j.ymeth.2014.03.009.
- Nagy S**, Tramm N, Sanders J, Iwanir S, Shirley IA, Levine E, Biron D. Homeostasis in *C. elegans* sleep is characterized by two behaviorally and genetically distinct mechanisms. *eLife*. 2014 Dec; 3:e04380. <https://elifesciences.org/articles/04380>, doi: 10.7554/eLife.04380.
- Nekimken AL**, Mazzochette EA, Goodman MB, Pruitt BL. Forces applied during classical touch assays for *Caenorhabditis elegans*. *PLOS ONE*. 2017 May; 12(5):e0178080. <http://journals.plos.org/plosone/article?id=10.1371/journal.pone.0178080>, doi: 10.1371/journal.pone.0178080.
- Nguyen JP**, Linder AN, Plummer GS, Shaevitz JW, Leifer AM. Automatically tracking neurons in a moving and deforming brain. *PLOS Computational Biology*. 2017 May; 13(5):e1005517. <http://journals.plos.org/ploscompbiol/article?id=10.1371/journal.pcbi.1005517>, doi: 10.1371/journal.pcbi.1005517.
- O'Hagan R**, Chalfie M, Goodman MB. The MEC-4 DEG/ENaC channel of *Caenorhabditis elegans* touch receptor neurons transduces mechanical signals. *Nature Neuroscience*. 2005 Jan; 8(1):43–50. <http://www.nature.com/neuro/journal/v8/n1/full/nn1362.html>, doi: 10.1038/nn1362.
- Petzold BC**, Park SJ, Mazzochette EA, Goodman MB, Pruitt BL. MEMS-based force-clamp analysis of the role of body stiffness in *C. elegans* touch sensation. *Integrative Biology*. 2013 May; 5(6):853–864. <http://pubs.rsc.org/en/content/articlelanding/2013/ib/c3ib20293c>, doi: 10.1039/C3IB20293C.
- Pirri JK**, Alkema MJ. The neuroethology of *C. elegans* escape. *Current Opinion in Neurobiology*. 2012 Apr; 22(2):187–193. <http://www.sciencedirect.com/science/article/pii/S095943881100225X>, doi: 10.1016/j.conb.2011.12.007.
- Porto DA**, Giblin J, Zhao Y, Lu H. Reverse-Correlation Analysis of Mechanosensation Circuit in *C. elegans* Reveals Temporal and Spatial Encoding. *bioRxiv*. 2017 Aug; <http://biorxiv.org/content/early/2017/08/07/147363>. abstract, doi: 10.1101/147363.
- Ramot D**, Johnson BE, Berry TL Jr, Carnell L, Goodman MB. The Parallel Worm Tracker: A Platform for Measuring Average Speed and Drug-Induced Paralysis in Nematodes. *PLoS ONE*. 2008 May; 3(5):e2208. <http://dx.plos.org/10.1371/journal.pone.0002208>, doi: 10.1371/journal.pone.0002208.
- Rankin CH**, Wicks SR. Mutations of the *Caenorhabditis elegans* Brain-Specific Inorganic Phosphate Transporter eat-4 Affect Habituation of the Tap-Withdrawal Response without Affecting the Response Itself. *Journal of Neuroscience*. 2000 Jun; 20(11):4337–4344. <http://www.jneurosci.org/content/20/11/4337>.
- Rankin CH**, Beck CDO, Chiba CM. *Caenorhabditis elegans*: A new model system for the study of learning and memory. *Behavioural Brain Research*. 1990 Feb; 37(1):89–92. <http://www.sciencedirect.com/science/article/pii/016643289090074O>, doi: 10.1016/0166-4328(90)90074-O.
- Ringach D**, Shapley R. Reverse correlation in neurophysiology. *Cognitive Science*. 2004 Mar; 28(2):147–166. <http://www.sciencedirect.com/science/article/pii/S0364021303001174>, doi: 10.1016/j.cogsci.2003.11.003.
- Sanyal S**, Wintle RF, Kindt KS, Nuttley WM, Arvan R, Fitzmaurice P, Bigras E, Merz DC, Hébert TE, Kooy Dvd, Schaffer WR, Culotti JG, Tol HHMV. Dopamine modulates the plasticity of mechanosensory responses in *Caenorhabditis elegans*. *The EMBO Journal*. 2004 Jan; 23(2):473–482. <http://emboj.embopress.org/content/23/2/473>, doi: 10.1038/sj.emboj.7600057.
- Schwartz O**, Pillow JW, Rust NC, Simoncelli EP. Spike-triggered neural characterization. *Journal of Vision*. 2006 Jul; 6(4):484–507. doi: 10.1167/6.4.13.

- Schwarz J**, Lewandrowski I, Bringmann H. Reduced activity of a sensory neuron during a sleep-like state in *Caenorhabditis elegans*. *Current Biology*. 2011 Dec; 21(24):R983–R984. <http://www.sciencedirect.com/science/article/pii/S0960982211012073>, doi: 10.1016/j.cub.2011.10.046.
- Stephens GJ**, Johnson-Kerner B, Bialek W, Ryu WS. Dimensionality and Dynamics in the Behavior of *C. elegans*. *PLoS Computational Biology*. 2008 Apr; 4(4):e1000028. <http://dx.doi.org/10.1371/journal.pcbi.1000028>, doi: 10.1371/journal.pcbi.1000028.
- Stirman JN**, Crane MM, Husson SJ, Wabnig S, Schultheis C, Gottschalk A, Lu H. Real-time multimodal optical control of neurons and muscles in freely behaving *Caenorhabditis elegans*. *Nature methods*. 2011 Feb; 8(2):153–158. <http://www.ncbi.nlm.nih.gov/pubmed/21240278>, doi: 10.1038/nmeth.1555.
- Swierczek NA**, Giles AC, Rankin CH, Kerr RA. High-throughput behavioral analysis in *C. elegans*. *Nature Methods*. 2011 Jun; 8(7):592. <https://www.nature.com/articles/nmeth.1625>, doi: 10.1038/nmeth.1625.
- Timbers TA**, Giles AC, Ardiel EL, Kerr RA, Rankin CH. Intensity discrimination deficits cause habituation changes in middle-aged *Caenorhabditis elegans*. *Neurobiology of Aging*. 2013 Feb; 34(2):621–631. <http://www.sciencedirect.com/science/article/pii/S0197458012002291>, doi: 10.1016/j.neurobiolaging.2012.03.016.
- Wicks SR**, Rankin CH. Integration of mechanosensory stimuli in *Caenorhabditis elegans*. *Journal of Neuroscience*. 1995 Mar; 15(3):2434–2444. <http://www.jneurosci.org/content/15/3/2434>.
- Wiltschko A**, Johnson M, Iurilli G, Peterson R, Katon J, Pashkovski S, Abraira V, Adams R, Datta S. Mapping Sub-Second Structure in Mouse Behavior. *Neuron*. 2015 Dec; 88(6):1121–1135. <http://www.sciencedirect.com/science/article/pii/S0896627315010375>, doi: 10.1016/j.neuron.2015.11.031.
- Yemini E**, Jucikas T, Grundy LJ, Brown AEX, Schafer WR. A database of *Caenorhabditis elegans* behavioral phenotypes. *Nature Methods*. 2013 Jul; 10(9):877. <https://www.nature.com/articles/nmeth.2560>, doi: 10.1038/nmeth.2560.
- Yilmaz M**, Meister M. Rapid Innate Defensive Responses of Mice to Looming Visual Stimuli. *Current Biology*. 2013 Oct; 23(20):2011–2015. <http://www.sciencedirect.com/science/article/pii/S0960982213009913>, doi: 10.1016/j.cub.2013.08.015.

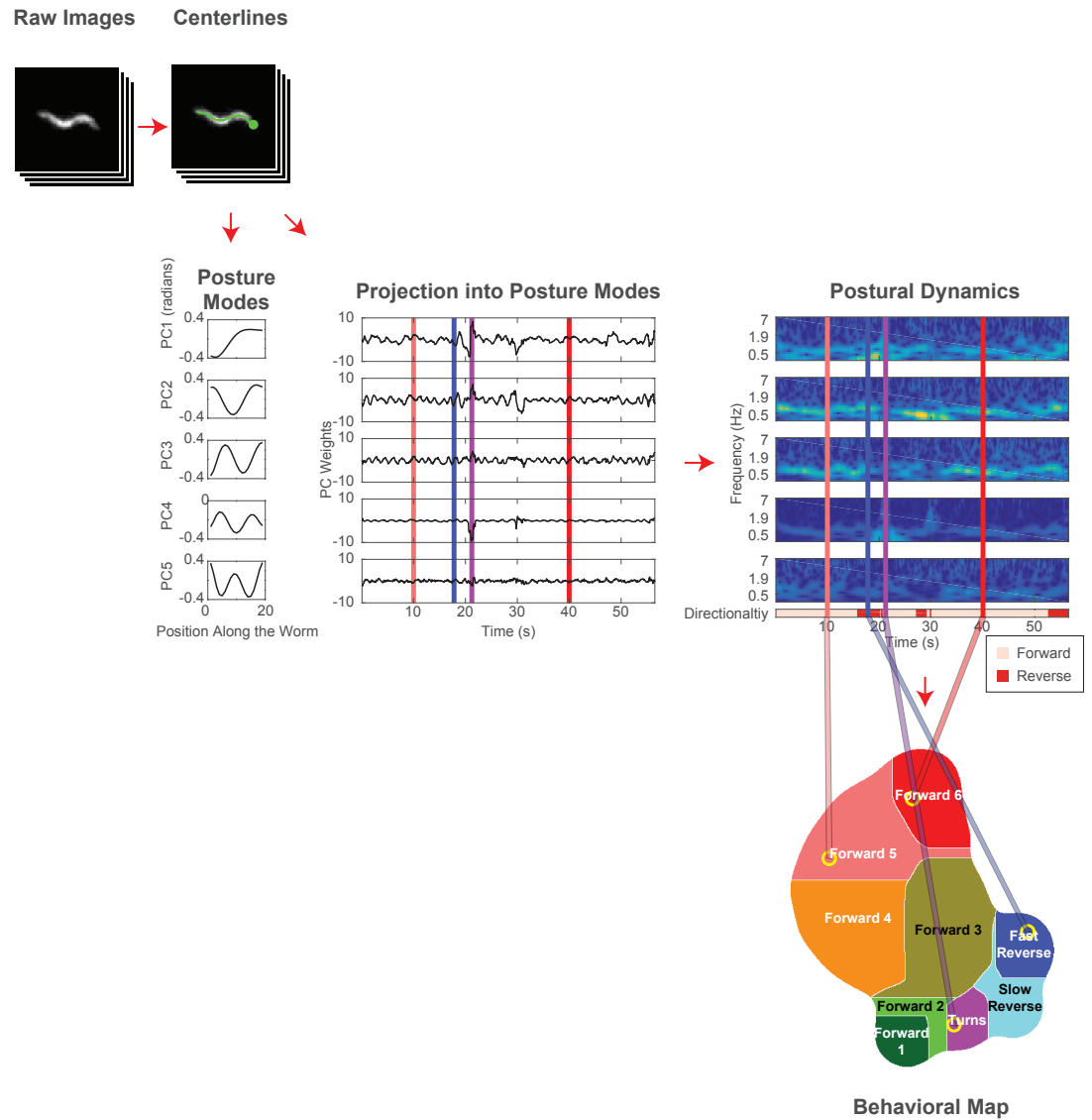


Figure 1-Figure supplement 1. Analysis pipeline for classifying behavior. Behavior is mapped and classified according to the animal's posture dynamics, similar to in (Berman *et al.*, 2014). Images of *C. elegans* are segmented to extract the animal's centerline. Each centerline is projected into a linear combination of posture modes. The animal's time-varying posture is represented as a time-series of corresponding weights. Spectrograms of these time-series describe the animal's postural dynamics at each point in time. Posture dynamics are mapped into a two-dimensional plane using t-SNE. The animal occupies a different point on the behavior map depending on its postural dynamics, and its placement in this map determines the behavioral classification.

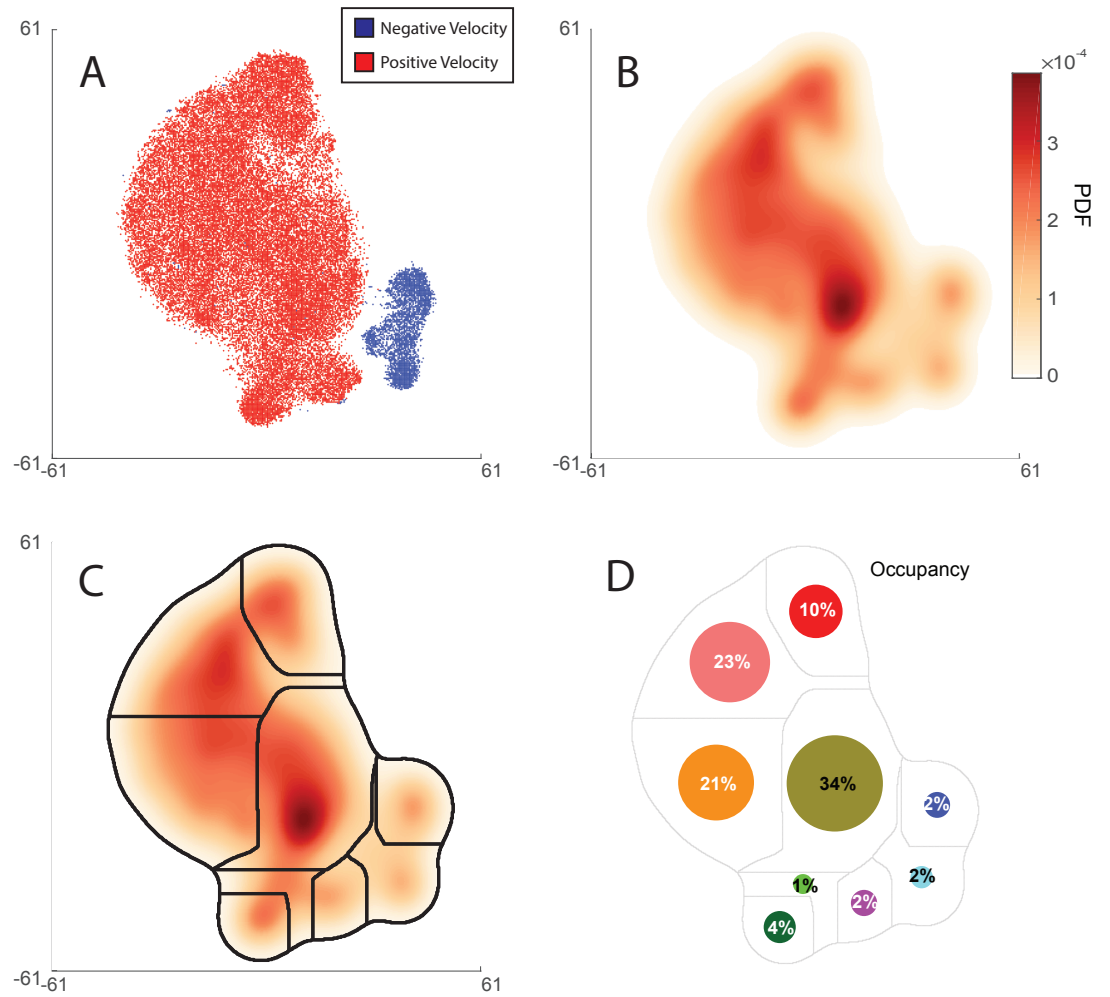


Figure 1-Figure supplement 2. Behavior map details. Behavior maps were generated from 2,284 animal-hours of behavior recorded from *Pmec-4::Chrimson* worms during optogenetic stimulation and control conditions. a) The sign of the animal's velocity is shown for 55,000 time-points uniformly selected from the recordings. Distinct regions in the map correspond to forward or backward locomotion. b) Probability density plot shows likelihood that the animal exhibits different behaviors. Peaks in the probability density correspond to stereotyped behaviors. c) Natural boundaries that separate stereotyped worm behaviors are found using watershedding. Same as in **Figure 1**. These regions define distinct behavior states. d) The probability of occupying a given behavior is shown for animals in an unstimulated condition. Area of circle scales with occupancy probability.

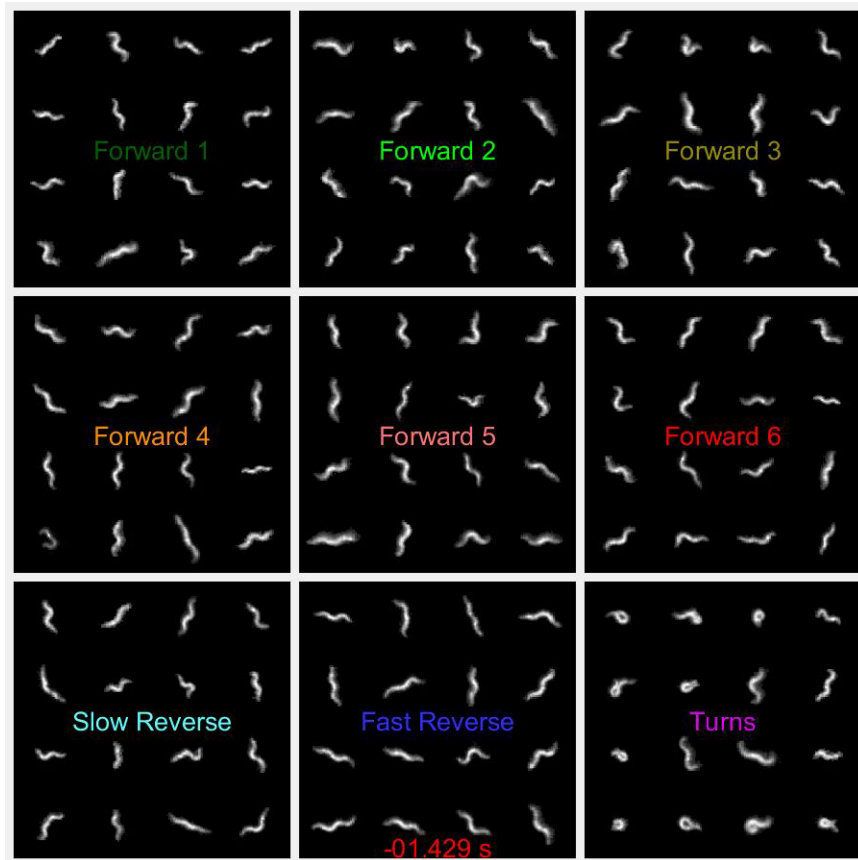


Figure 1-Figure supplement 3. Videos of randomly selected animals performing each of the 9 behaviors. Randomly selected 3-second long examples of animals performing each of the 9 behaviors. Link to video (<https://vimeo.com/259479020>)

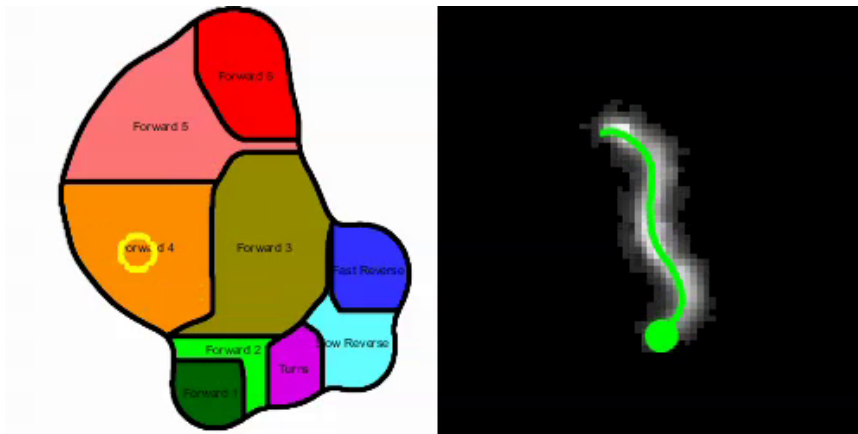


Figure 1-Figure supplement 4. Video showing path of an animal through behavior space. **right.)** Video of an example animal is shown. Detected centerline (green) is overlaid. Dot denotes head. The animal is kept centered in the video, even though it is moving. **left.)** Animal's instantaneous behavior is shown (yellow ring) on the behavioral map. Link to video (<https://vimeo.com/259479010>)

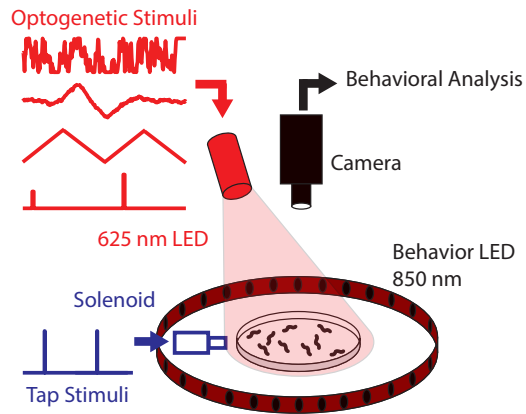


Figure 2-Figure supplement 1. Diagram of high-throughput stimulation and behavior assay. Worm behavior is recorded while delivering optogenetic or tap stimulation to a plate containing 6340 animals (mean \pm standard deviation). Optogenetic stimulation is delivered by modulating the light intensity of three 625nm LEDs (only one is shown in the diagram). Taps are delivered to the plate via a computer controlled solenoid. Recordings last 30 minutes per plate, and each experimental series consists of many plates, see **Table 2**.

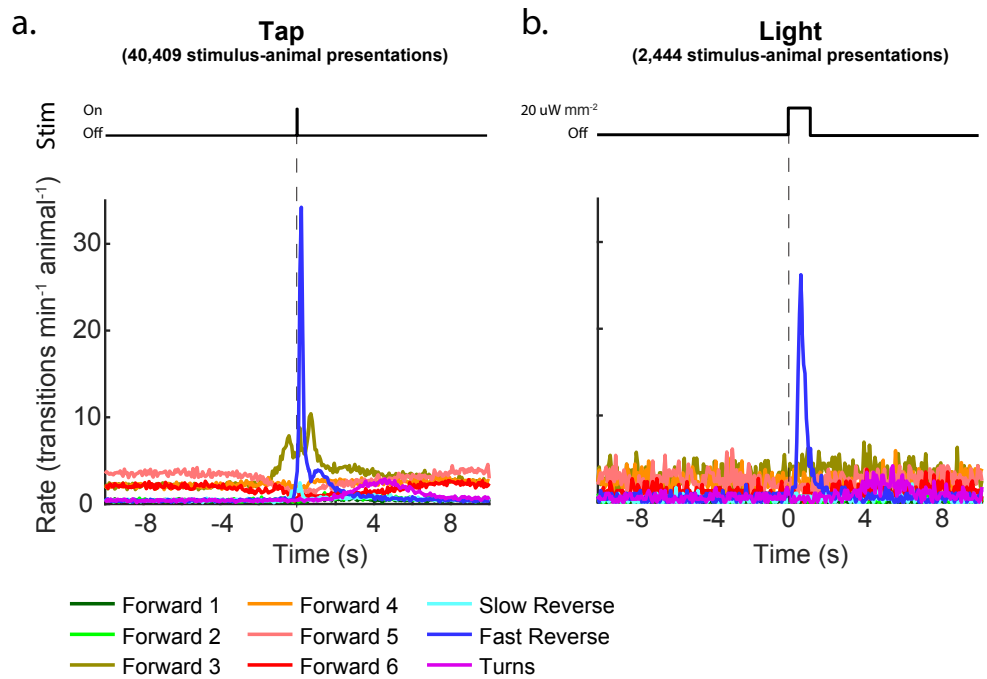


Figure 2-Figure supplement 2. Transition rates for tap and light stimulation. The rate of transitions into each behavior is shown aligned to a tap or 1 s optogenetic light stimulus. Panels **a** and **b** correspond to the occupancy plots in **Figure 2a** and **b**.

Light Control (- ATR) (1,329 stimulus-animal presentations)

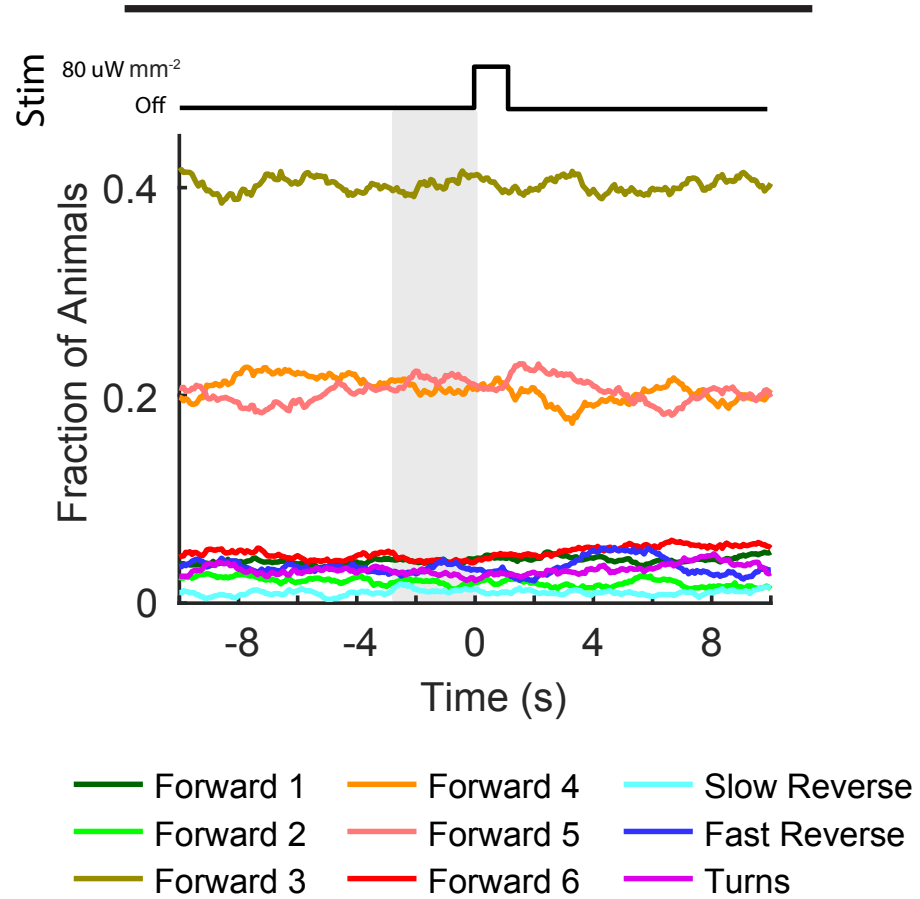


Figure 2-Figure supplement 3. Control animals grown without ATR are light insensitive. Fractions of control AML67 animals occupying each behavior state are shown in response to a light pulse stimulus. Animals grown without all-trans-retinal (- ATR) do not respond to light even at a light intensity level of $80 \mu\text{W mm}^{-2}$.

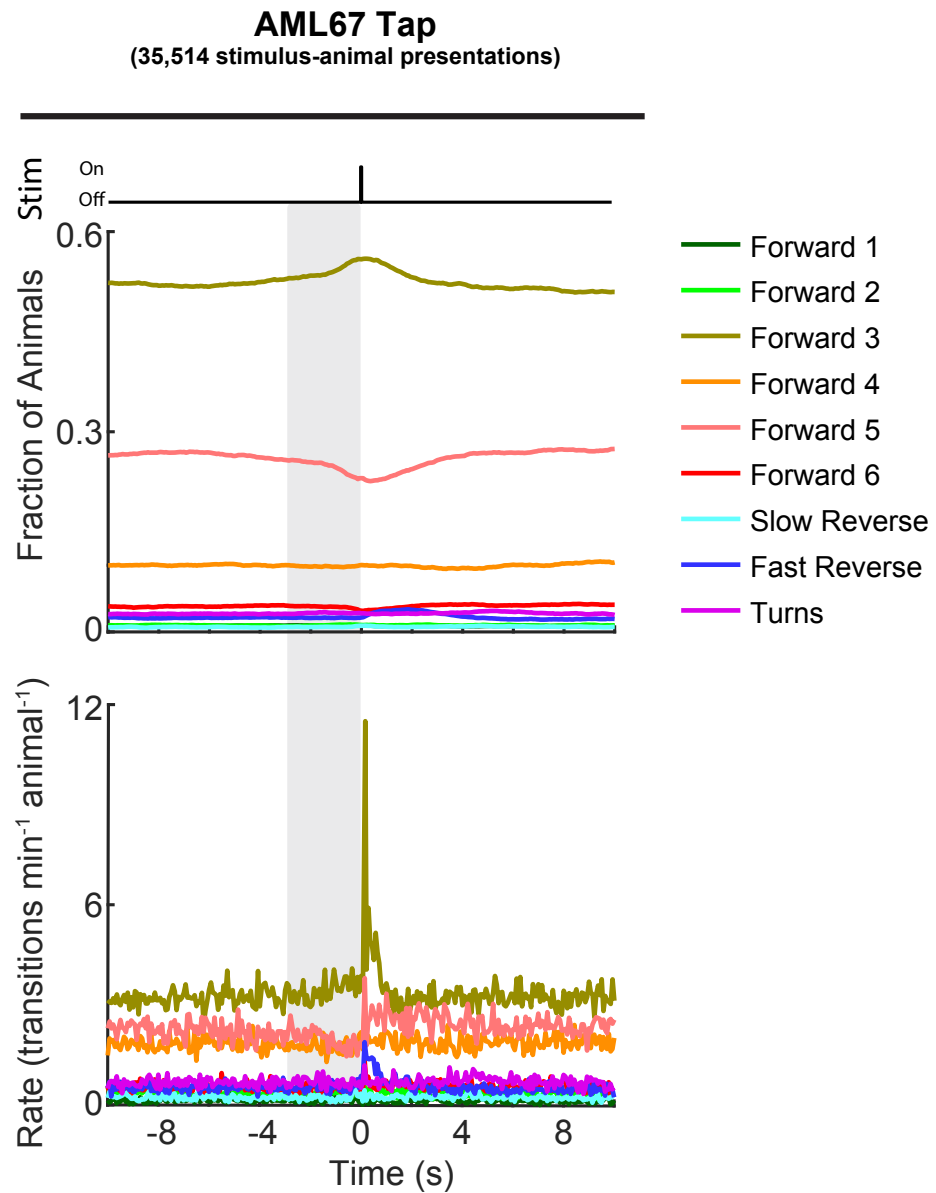


Figure 2-Figure supplement 4. Tap sensitivity of transgenic animals is reduced compared to wildtype. Fractions of AML67 animals occupying each behavior state and transition rates into each behavior are shown in response to a mechanical tap stimulus. Recordings from both ATR+ and ATR- conditions are pooled together. AML67 animals show decreased responsiveness to tap stimulation compared to wild-type presumably because the exogenous *mec-4* promoter sequences deplete the endogenous *mec-4* transcription factor.

Occupancy change between random noise stimulation and control
1,784 (stim) and 500 (control) animal-hours

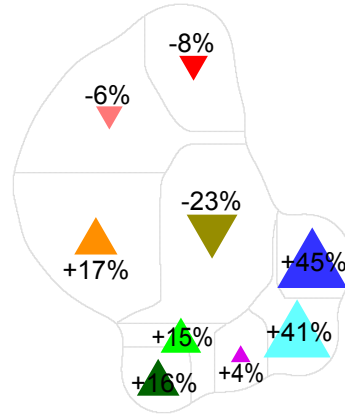


Figure 3-Figure supplement 1. Change in behavioral occupancy evoked by random noise stimulation. The change in occupancy during random noise optogenetic light stimulation (1,784 animal hours) compared to no-retinal control (500 animal-hours) is shown. Baseline occupancy during no-retinal control is shown in **Figure 1 - Figure Supplement 2d**.

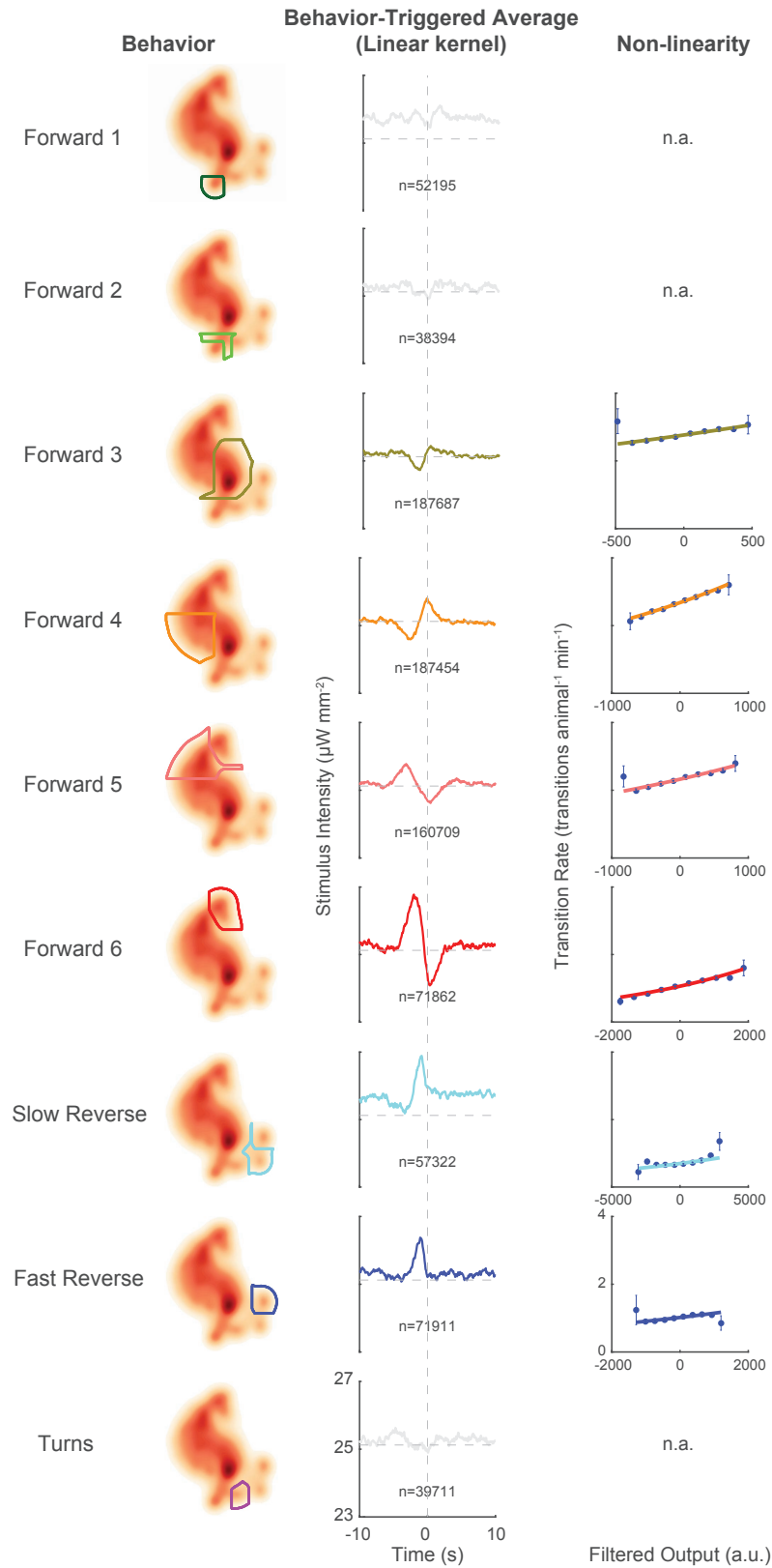


Figure 3-Figure supplement 2. Behavior triggered averages and non-linearities for all behaviors. Behavior triggered averages and associated non-linearities are shown for transitions into all 9 behavior states. Those behavior triggered averages that fail to pass a shuffled significance threshold are shown in light gray. Non-linearities are only calculated for behaviors whose behavior-triggered averages pass our shuffled significance test. Note that non-linearities are mostly well-approximated by a line, consistent with the observation in **Figure 2c** that the animal responds roughly linearly in our stimulus regime.

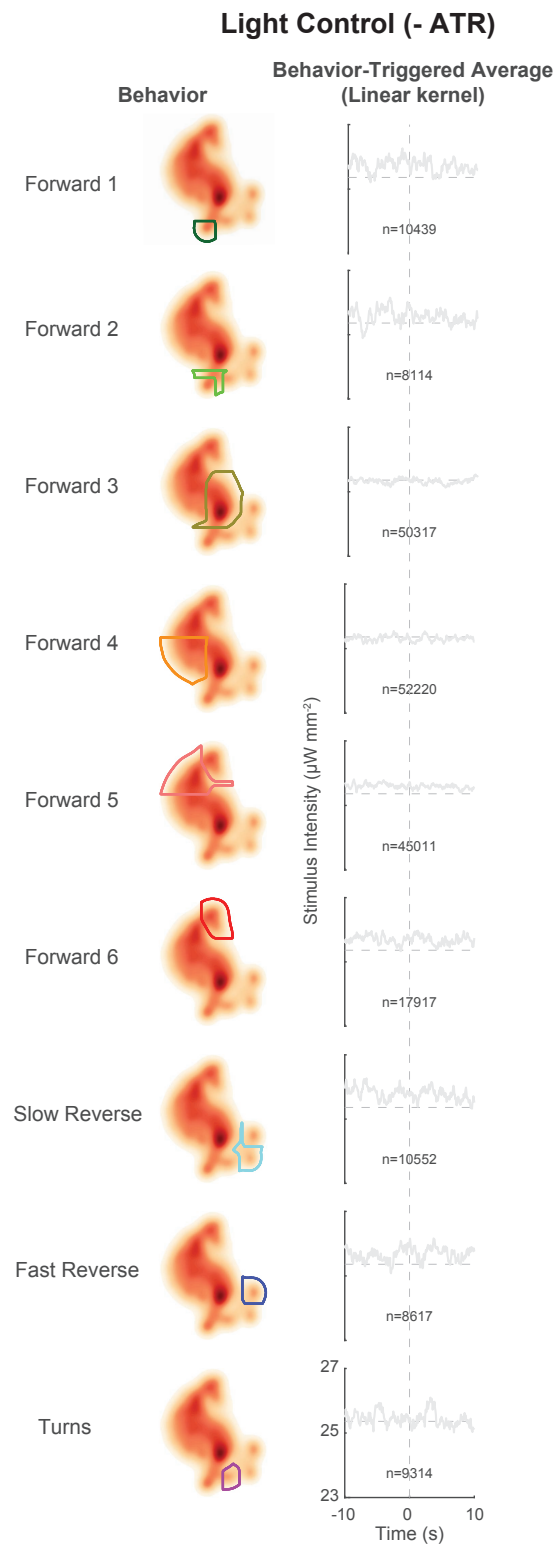


Figure 3-Figure supplement 3. Behavior triggered averages for control animals grown without ATR. Behavior triggered averages are shown for transitions into all 9 behavior states for control animals grown without the required cofactor all-trans retinal (ATR). As expected, none of the kernels pass a shuffled significance threshold. Consequently non-linearities were not calculated.

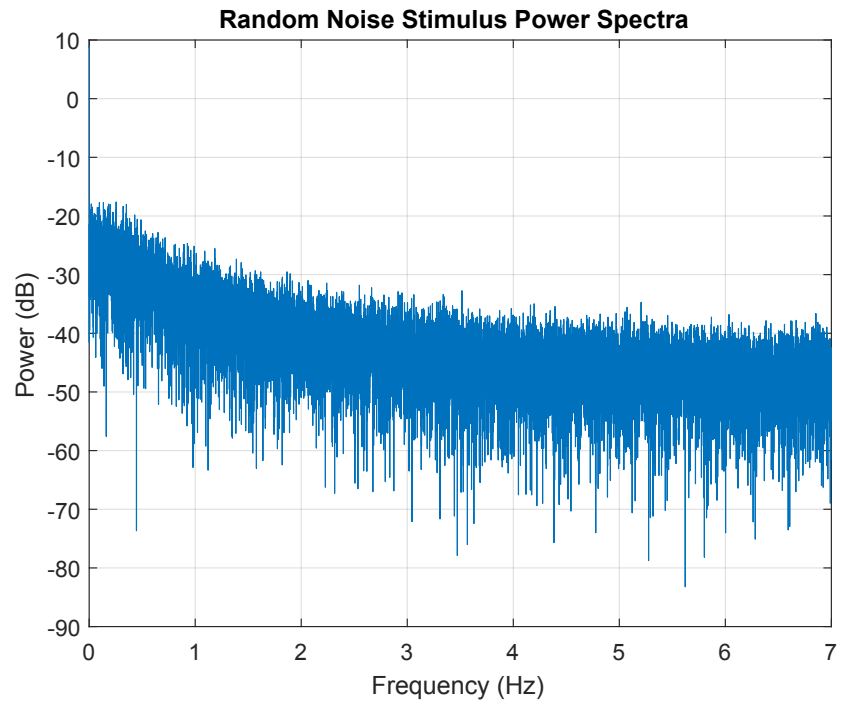


Figure 3-Figure supplement 4. Power spectra of a single instantiation of the random noise stimulus. The MATLAB periodogram function is used to generate the power spectra of the random noise stimulus for a 30 minute experiment.

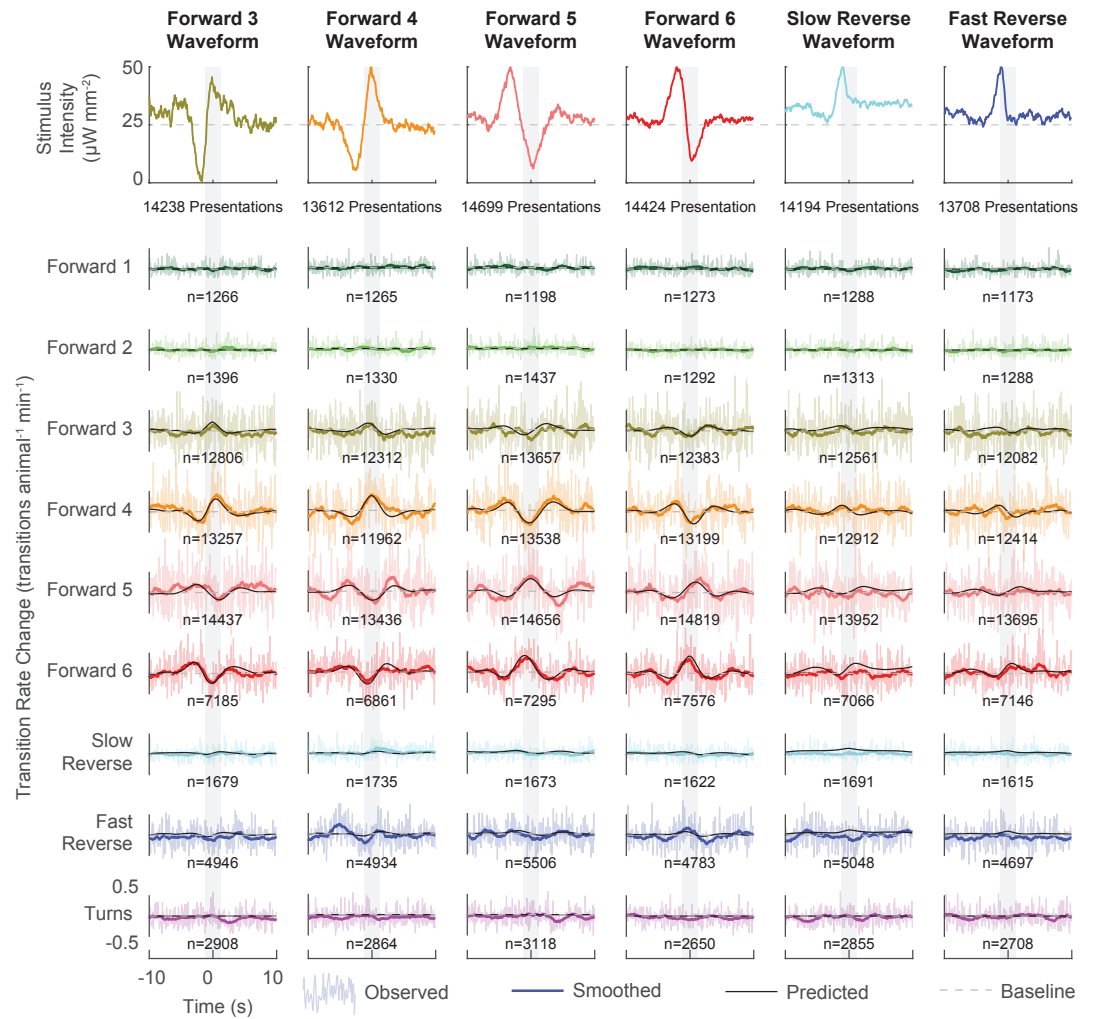


Figure 4-Figure supplement 1. Behavioral responses to all kernel-shaped stimuli. The LN model predicts the transition rate change from baseline for the nine behaviors in response to six stimuli constructed from statistically significant behavior triggered averages. n refers to the number of transitions of the corresponding behavior observed during the 20 second window. Presentation numbers refer to stimulus-animal presentations.

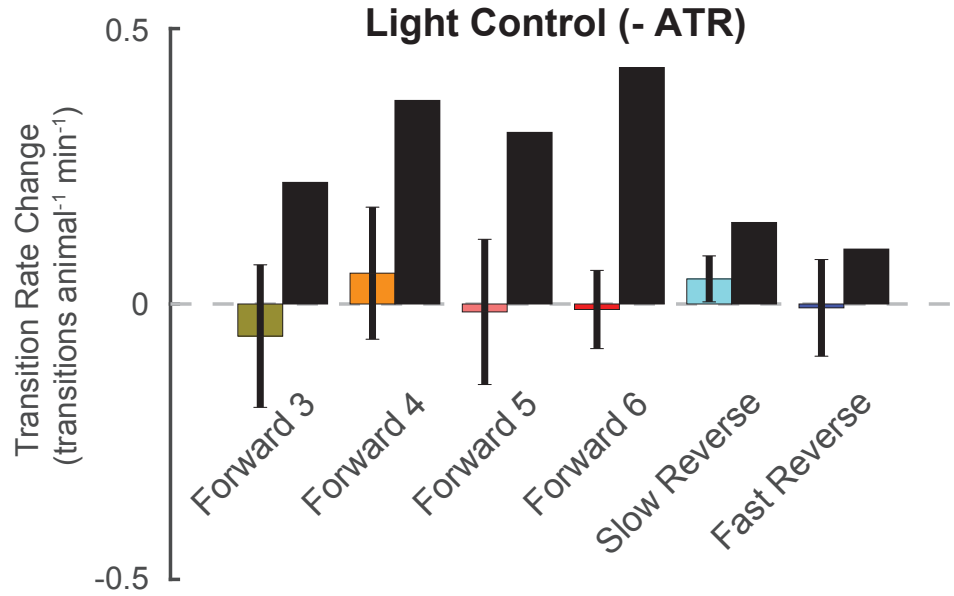


Figure 4–Figure supplement 2. Control animals grown without ATR do not respond to kernel-shaped stimulus. Kernel-shaped stimuli are delivered to AML67 control animals grown without the required co-factor ATR. The change in transition rate into the kernel-shaped stimuli's corresponding behavior is shown, as in Figure 4a. Control animals do not exhibit a significant increase in transitions into the expected behavior states. Error bars show standard error of the mean. Black bars show LN predictions for light sensitive animals. The number of stimulus-animal presentations, from left to right, were {3,474, 3,880, 3,988, 3,639, 4,351, 3,534.}. Of these, the number of timely transitions were {355, 225, 396, 162, 68, 95.}. The p-values from a t-test were {0.63, 0.97, 0.92, 0.87, 0.33, 0.68.}

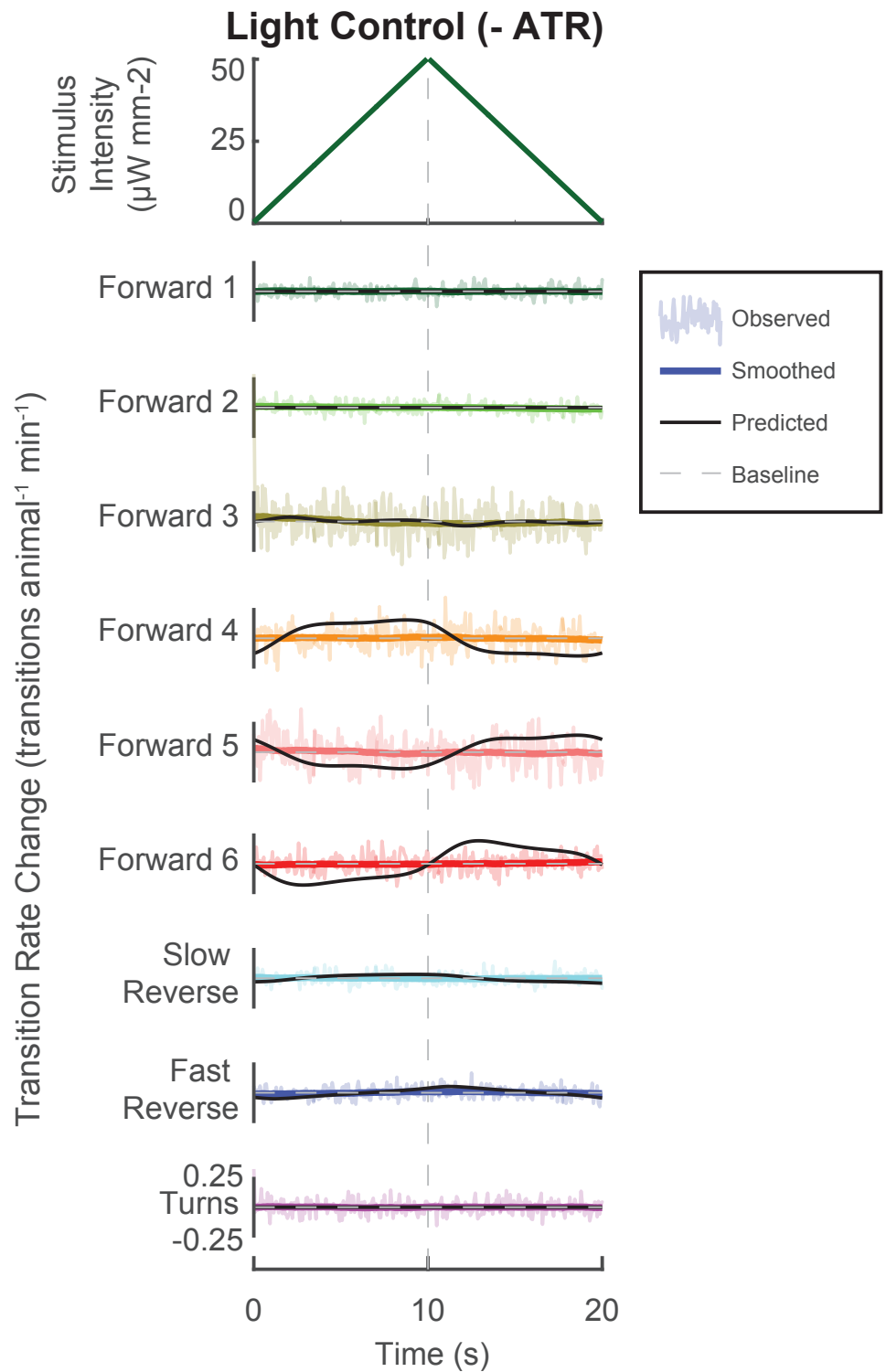


Figure 5-Figure supplement 1. Control animals grown without ATR do not respond to triangle wave stimuli. A novel triangle-wave optogenetic light stimulus, as in **Figure 5**, was repeatedly presented to control animals grown without the required co-factor retinal. Control animals do not respond to the stimulus. Observed response is shown as well as LN predicted response for light-sensitive animals. Of 142,461 animal-stimulus presentations the following number of transitions were observed (by row, from top to bottom): {14,575, 15,886, 146,149, 82,216, 131,060, 42,080, 16,871, 18,581, 28,318}.

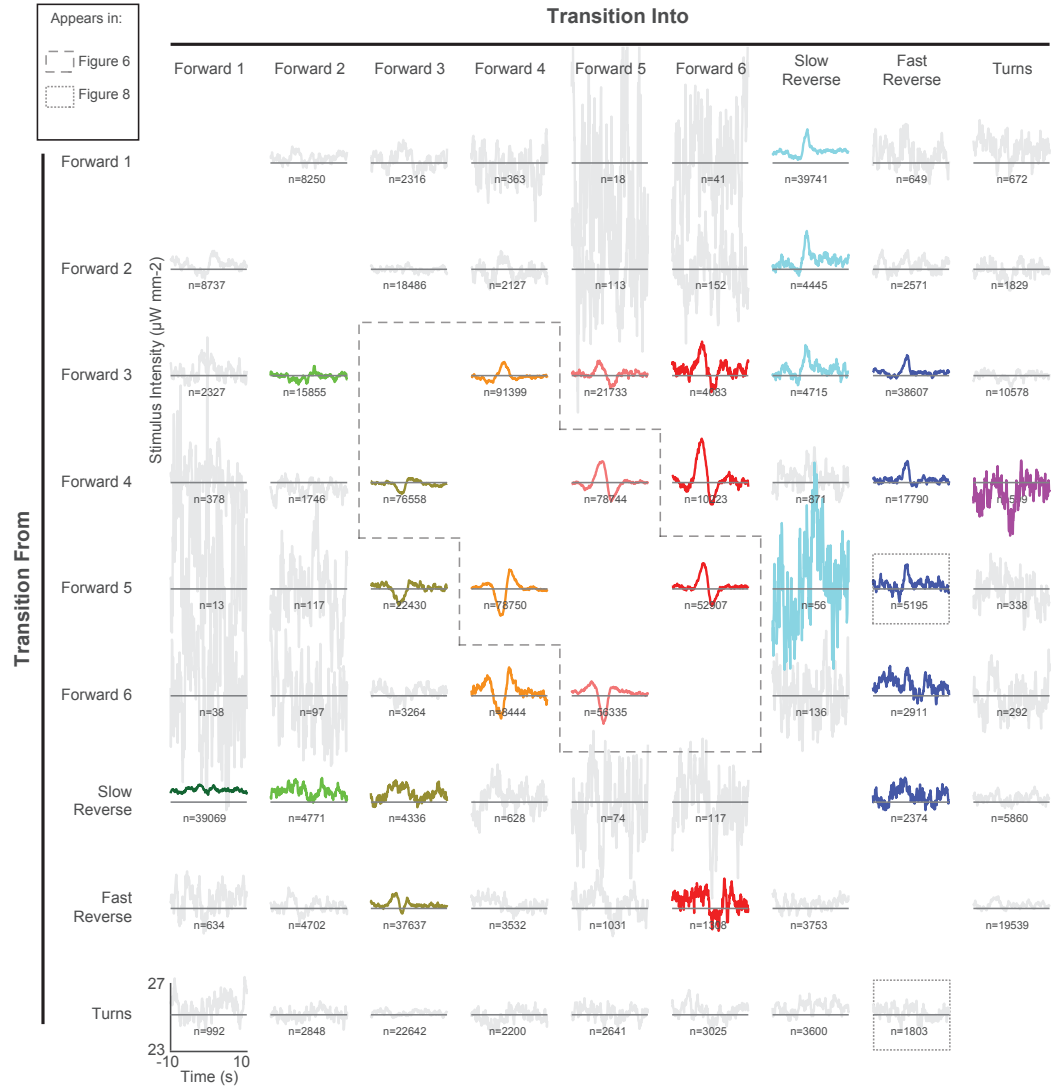


Figure 6-Figure supplement 1. All 72 pairwise context-dependent behavior triggered averages. Pairwise behavior triggered averages (also referred to as kernels) are shown for transitions from one specified behavior to another. Kernels are calculated from 1,784 animal-hours of continuous random noise stimulation, same as in **Figure 3**. For transitions into a given behavior (column), the kernel waveforms differ depending on the behavior that the animal originated in (rows). This suggests that the animal's behavioral response to stimulus depends on the animal's current behavior state. For each kernel, the vertical axis spans 23 to 27 $\mu\text{W mm}^{-2}$ and horizontal axis spans -10 to 10 seconds. *n* indicates number of transitions observed. Kernels that fail to pass a shuffled significance threshold are grayed out (see methods).

Light Control (- ATR)

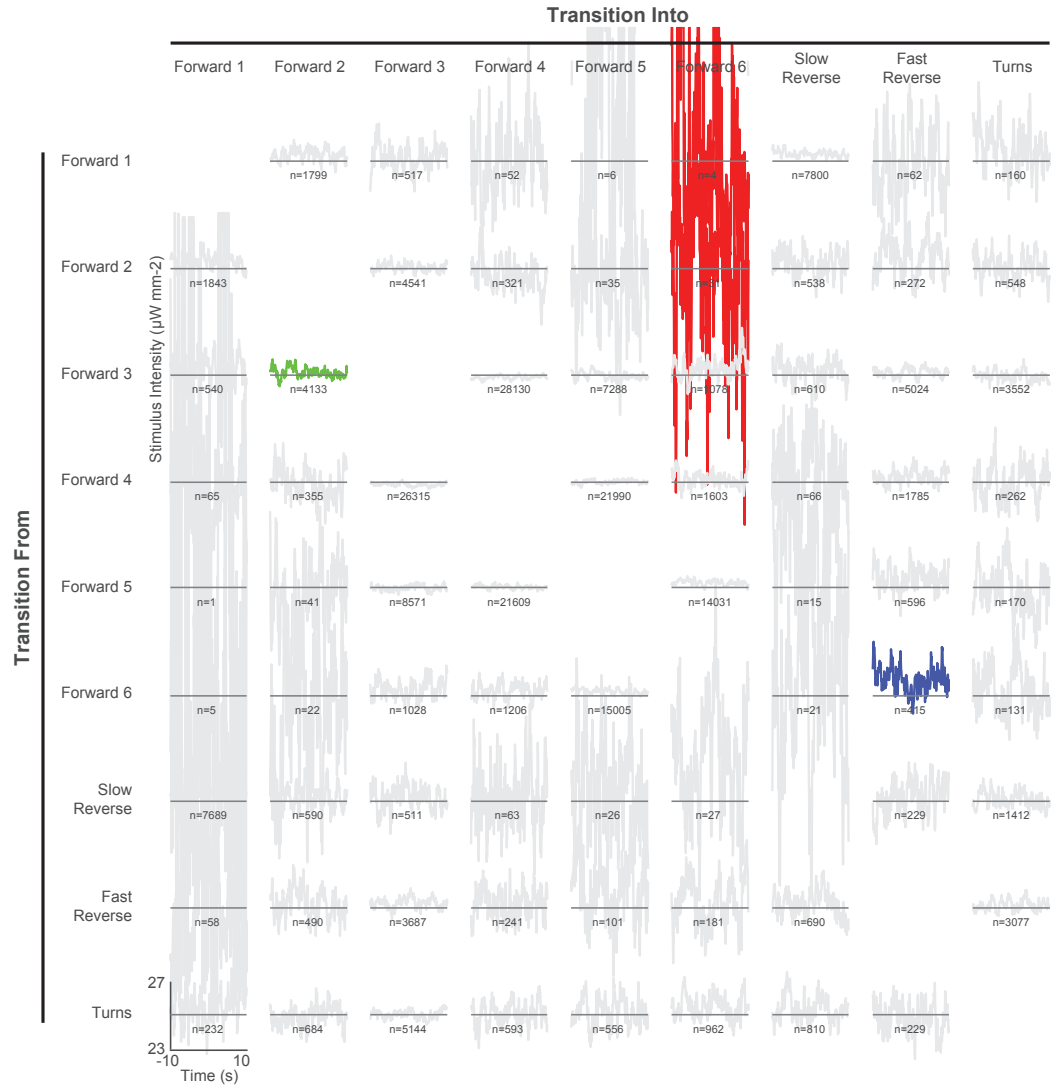


Figure 6-Figure supplement 2. All 72 pairwise context-dependent behavior triggered averages for control animals grown without ATR. Pairwise behavior triggered averages (also referred to as kernels) are shown for transitions from one specified behavior to another. For each kernel, the vertical axis spans 23 to 27 $\mu\text{W mm}^{-2}$ and horizontal axis spans -10 to 10 seconds. *n* indicates number of transitions observed. Kernels that fail to pass a shuffled significance threshold are grayed out (see methods).



Figure 8-Figure supplement 1. Transition rates in response to light pulse for all pairwise transitions. Transition rate is shown for all observed pairwise transitions in response to 1 s light pulse (+, right bar, 2,487 stimulus-animal presentations) and mock control (-, left bar, 2,427 stimulus-animal presentations). Number of observed transitions n for each bar is listed. No bars are shown for pairwise transitions that were not observed. Red square and star indicate significance, calculated by a multiple hypothesis corrected E-test, see methods. P-values are listed in **Figure 8 - Figure supplement 2**. Note that y axis range is 0 to 2 transitions animal⁻¹ min⁻¹ for all cases except for Forward 3→Fast Reverse, where it is 0 to 6 transitions animal⁻¹ min⁻¹.

	Forward 1	Forward 2	Forward 3	Forward 4	Forward 5	Forward 6	Slow Reverse	Fast Reverse	Turn
Forward 1		$8.65 \cdot 10^{-1}$					$3.17 \cdot 10^{-2}$		
Forward 2	$1.85 \cdot 10^{-1}$		$3.30 \cdot 10^{-1}$				$4.77 \cdot 10^{-1}$	$8.65 \cdot 10^{-1}$	
Forward 3	$4.82 \cdot 10^{-1}$	$3.73 \cdot 10^{-1}$		$2.17 \cdot 10^{-3}$	$3.24 \cdot 10^{-3}$	$4.13 \cdot 10^{-2}$	$9.66 \cdot 10^{-3}$	0	$4.91 \cdot 10^{-1}$
Forward 4		$8.65 \cdot 10^{-1}$	$1.42 \cdot 10^{-6}$		$1.97 \cdot 10^{-6}$	$8.65 \cdot 10^{-1}$	$8.84 \cdot 10^{-2}$	0	
Forward 5			$3.56 \cdot 10^{-1}$	$4.89 \cdot 10^{-3}$		$4.23 \cdot 10^{-7}$		$1.96 \cdot 10^{-9}$	
Forward 6			$1.85 \cdot 10^{-2}$	$5.94 \cdot 10^{-2}$	$9.53 \cdot 10^{-9}$			0	
Slow Reverse	$7.52 \cdot 10^{-1}$	$8.65 \cdot 10^{-1}$	$4.82 \cdot 10^{-1}$	$8.65 \cdot 10^{-1}$				$4.82 \cdot 10^{-1}$	$7.37 \cdot 10^{-1}$
Fast Reverse		$4.82 \cdot 10^{-1}$	$7.17 \cdot 10^{-2}$	$4.82 \cdot 10^{-1}$	$4.82 \cdot 10^{-1}$	$1.37 \cdot 10^{-6}$	$9.08 \cdot 10^{-1}$		$1.65 \cdot 10^{-1}$
Turns			$6.75 \cdot 10^{-1}$			$4.82 \cdot 10^{-1}$	$7.27 \cdot 10^{-1}$	$6.81 \cdot 10^{-1}$	

Figure 8-Figure supplement 2. P-values for transition rates in response to light pulse for all pairwise transitions. P-values are listed for the multiple hypothesis corrected E-tests performed in **Figure 8 - Figure Supplement 1**. Row specifies “transition from” and column specifies “transition into.”



Figure 8-Figure supplement 3. Transition rates in response to tap for all pairwise transitions. Transition rate is shown for all observed pairwise transitions in response to tap (+, right bar, 37,000 stimulus-animal presentations) and mock control (-, left bar, 40,012 stimulus-animal presentations). Number of observed transitions n for each bar is listed. No bars are shown for pairwise transitions that were not observed. Red square and star indicate significance, calculated by a multiple hypothesis corrected E-test, see methods. P-values are listed in **Figure 8 - Figure supplement 4**. All y axis range is 0 to 2 transitions animal⁻¹ min⁻¹.

	Forward 1	Forward 2	Forward 3	Forward 4	Forward 5	Forward 6	Slow Reverse	Fast Reverse	Turn
Forward 1		$7.98 \cdot 10^{-4}$	$2.60 \cdot 10^{-1}$	$4.82 \cdot 10^{-1}$			$1.99 \cdot 10^{-5}$		$4.18 \cdot 10^{-2}$
Forward 2	$9.97 \cdot 10^{-2}$		$2.94 \cdot 10^{-1}$	$1.47 \cdot 10^{-1}$		$4.82 \cdot 10^{-1}$	$3.48 \cdot 10^{-2}$	$8.43 \cdot 10^{-4}$	$8.27 \cdot 10^{-2}$
Forward 3	$4.20 \cdot 10^{-3}$	0		$4.58 \cdot 10^{-1}$	$6.54 \cdot 10^{-1}$	$9.61 \cdot 10^{-2}$	$9.59 \cdot 10^{-9}$	0	$5.95 \cdot 10^{-3}$
Forward 4	$1.25 \cdot 10^{-1}$	$3.92 \cdot 10^{-2}$	0		0	$3.84 \cdot 10^{-5}$	$1.02 \cdot 10^{-4}$	0	$2.03 \cdot 10^{-1}$
Forward 5	$4.82 \cdot 10^{-1}$	$5.78 \cdot 10^{-2}$	$3.36 \cdot 10^{-2}$	0		0		0	$4.75 \cdot 10^{-1}$
Forward 6	$4.82 \cdot 10^{-1}$	$4.18 \cdot 10^{-2}$	0	$3.17 \cdot 10^{-3}$	0		$1.25 \cdot 10^{-1}$	0	$2.03 \cdot 10^{-1}$
Slow Reverse	$4.61 \cdot 10^{-12}$	$3.83 \cdot 10^{-3}$	$2.60 \cdot 10^{-6}$	$4.82 \cdot 10^{-1}$		$4.82 \cdot 10^{-1}$		$1.62 \cdot 10^{-2}$	$4.14 \cdot 10^{-1}$
Fast Reverse	$4.82 \cdot 10^{-1}$	$4.09 \cdot 10^{-1}$	$1.37 \cdot 10^{-5}$	$2.32 \cdot 10^{-2}$	$2.98 \cdot 10^{-2}$	$6.17 \cdot 10^{-14}$	$9.38 \cdot 10^{-1}$		$4.70 \cdot 10^{-1}$
Turns	$4.20 \cdot 10^{-1}$	$2.28 \cdot 10^{-1}$	$8.31 \cdot 10^{-2}$	$1.13 \cdot 10^{-1}$	$6.33 \cdot 10^{-2}$	$2.46 \cdot 10^{-1}$	$3.57 \cdot 10^{-2}$	$3.40 \cdot 10^{-1}$	

Figure 8-Figure supplement 4. P-values for transition rates in response to tap for all pairwise transitions. P-values are listed for the multiple hypothesis corrected E-tests performed in **Figure 8 - Figure Supplement 3**. Row specifies “transition from” and column specifies “transition into.”